Development of a physiologically based toxicokinetic model for lead in pregnant women: The role of bone tissue in the maternal and fetal internal exposure

Y. Ali Daoud, C. Tebby, R. Beaudouin, C. Brochot

Development of a physiologically based toxicokinetic model for lead in pregnant women: the role of bone tissue in the maternal and fetal internal exposure

Ali Daoud Y[1, 2], Tebby C[1*], Beaudouin R[1, 3] and Brochot C[1, 4]

[1]Experimental toxicology and modeling unit (MIV/TEAM), Institut National de l'Environnement Industriel et des Risques, 60550 Verneuil-en-Halatte, France

[2]Péritox, UMR-I 01, University of Picardie Jules Verne, 80025 Amiens, France

[3]Sebio, Experimental and modeling unit, UMR-I 02

[4]Certara UK Ltd, Simcyp Division, Sheffield, UK

*Corresponding author: cleo.bodin@ineris.fr

Highlights

- A PBPK model for lead was extended to pregnancy and fetal development
- Maternal bone remodeling increases blood lead levels in the 2nd and 3rd trimesters
- Ossification in the fetus induces a decrease in the exposure of the other organs
- A high inter-individual variability was estimated for the placental transfer rates

Abstract

Epidemiological studies have shown associations between prenatal exposure to lead (Pb) and neurodevelopmental effects in young children. Prenatal exposure is generally characterized by measuring the concentration in the umbilical cord at delivery or in the maternal blood during pregnancy. To assess internal Pb exposure during prenatal life, we developed a pregnancy physiologically based pharmacokinetic (p-PBPK) model that to simulates Pb levels in blood and target tissues in the fetus, especially during critical periods for brain development. An existing Pb PBPK model was adapted to pregnant women and fetuses. Using data from literature, both the additional maternal bone remodeling, that causes Pb release into the blood, and the Pb placental transfers were estimated by Bayesian inference. Additional maternal bone remodeling was estimated to start at 21.6 weeks. Placental transfers were estimated between 4.6 and 283 L.day^{-1} at delivery with high interindividual variability. Once calibrated, the p-PBPK model was used to simulate fetal exposure to Pb. Internal fetal exposure greatly varies over the pregnancy with two peaks of Pb levels in blood and brain at the end of the 1st and 3rd trimesters. Sensitivity analysis shows that the fetal blood lead levels are affected by the maternal burden of bone Pb via maternal bone remodeling and by fetal bone formation at different pregnancy stages. Coupling the p-PBPK model with an effect model such as an adverse outcome pathway could help to predict the effects on children's neurodevelopment.

Keywords: p-PBPK model, lead, metal, pregnancy, bone remodeling, resorption, placental transfer, fetus exposure, Monte Carlo simulations, parameter estimation.

1 Introduction

Lead (Pb) is a public health concern due to adverse effects on humans, especially on children and fetuses [1, 2]. Most of the effects of Pb exposure are related to the development of the central nervous system (CNS), and of the renal and cardiac systems [1] in children and fetuses. Indeed, in addition to increasing premature birth rates and low birth weights, *in utero* exposure increases occurrence of inadequate intrauterine growth and cognitive impairments with damage to fine motor skills [1]. Furthermore, prenatal Pb exposure, even at blood lead levels (BLLs) below 50 µg/L [3, 4], can alter brain development and could lead to behavioral difficulties, learning disabilities and lower intellectual quotient (IQ) [5, 6]. Although Pb toxicity has been proven for several decades, decreasing exposure of the human populations to Pb is still a priority. Recently, a series of scientific and policy-related questions on Pb exposure and its health effects were opened by the European Human Biomonitoring Initiative (HBM4EU) [7]. In particular, the placental transfer of Pb during prenatal exposure needs to be better characterized. Government actions to limit human Pb exposure have reduced BLLs in the general population [4, 8, 9]. The French National Authority for Health gives recommendations to identify and manage Pb exposure and has proposed a maximum BLL of 50 µg/L with mandatory reporting for over-exposed women of childbearing age and children [10]. Understanding and quantifying Pb transfers to fetuses during pregnancy may help refining these recommendations.

Pb absorption in humans depends on several factors including the route of exposure, nutritional status, health and age of the individual [1, 11-14]. In adults, about 90% of Pb body burden is found in bones and teeth and about 73% in children [15]. Pb is mainly excreted in urine and bile [1] with a half-life in adults of about 30 days in blood and of 10 to 20 years in bone [16, 17]. However, the half-life of Pb in blood varies depending on age and duration of exposure. Thus, in children aged 1 to 4 years, the half-life of Pb in blood has been calculated to be between 10 months and 38 months [18]. Pb is a bone-seeking element that forms highly stable complexes with phosphate [19]. Pb is deposited in bones and can be released in blood due to bone remodeling process [20]. During pregnancy, the high fetal demand for calcium to form bones and teeth increases the maternal bone remodeling, especially during the 2nd and 3rd trimesters. During pregnancy, Pb in bones is

mobilized and released in the blood circulation. Such a release can contribute to increase the BLLs of pregnant women up to 88% during the 2nd trimester [21-25], leading to U-shaped pattern of BLLs [21, 26, 27]. Fetal Pb exposure is driven by a combination of factors, such as the passage of Pb through the placental barrier, the maternal internal exposure, and the Pb kinetics in the developing fetus. Several studies have shown that the BLLs in the mother and the fetus (umbilical cord at delivery) are positively correlated [28-31]. Gulson *et al.* [32] also showed that approximately 80% of Pb in cord blood at delivery originates from maternal bone Pb. Because Pb accumulates in bone, ossification in the fetus may also impact the Pb kinetics as this process is not continuous over pregnancy and begins between the 7th and 13th week after fertilization of the ovum [33, 34].

Fetal exposure throughout pregnancy remains uncertain since the only exposure data available are often the Pb levels in cord blood at delivery. Physiologically based pharmacokinetic or toxicokinetic modeling (PBPK/PBTK) is a powerful tool for simulating the concentrations of xenobiotics in living organisms over a time period. Such models integrate data to describe the absorption, distribution, metabolism and excretion (ADME) of compounds [35]. The potential impact of age-specific or population-specific characteristics on the internal exposure in blood and organs can be accounted for by integrating specific physiological and biochemical data in those models. PBPK models are increasingly used to improve risk assessment and drug development for sensitive populations including pregnant women and children [36-40]. Physiological changes in pregnant women and fetuses such as increased hematocrit, cardiac output, glomerular filtration, and organ volumes can impact the compound's ADME [41]. Including these changes in PBPK models allow to understand the impact of those changes on compound kinetics in pregnant women and to predict the internal exposure of fetuses [42, 43].

Several kinetic models for Pb in humans have been published, notably the Leggett model [44], the O'Flaherty model [20], and the AALM (All-Ages Lead Model) model [45]. All three models describe Pb disposition in blood and several organs from birth to adulthood. Leggett's model was used, among others, to determine the doses of Pb isotopes in chronically exposed people. In that model, Pb transfers between organs are not related to physiological processes, unlike in the O'Flaherty model. The latter integrates body weight and age dependent

physiological parameters (*e.g.,* organ blood flows and volumes). Another difference between these two models is the description of the structure and the Pb exchanges in bones. Bone-to-blood mobilization modeled with physiological processes is only integrated in the O'Flaherty model. The AALM model was recently developed and is based on both the O'Flaherty and Leggett models. A multimedia exposure model was also added to account for several exposure sources and routes. Combined with an exposure assessment, these kinetic models can be used to simulate BLL and internal tissue exposure in populations. Recently, the O'Flaherty PBPK model was used by Sy *et al.* [46] to set up an integrative modeling framework to assess the long-term exposure to Pb of the general population in four European countries. Their model was designed to account for the effect of past and current exposures to predict Pb levels until the 2070s. Another recent application is the study by Tebby *et al.* [47] that estimated the BLL in children at several ages in France using spatialized exposure data.

In this paper, we propose to extend the PBPK model for Pb developed by O'Flaherty to pregnant women and their fetuses. The anatomical and physiological changes during pregnancy were integrated. In particular, the additional bone remodeling in pregnant women and the ossification in the fetus were modelled based on published data. The placental transfers between the woman and the fetus and the parameters of additional bone remodeling in women were estimated by Bayesian inference. The pregnancy PBPK (p-PBPK) model was then evaluated using sensitivity analysis and by comparing the predicted ratio of cord blood lead level over maternal BLL with data from the literature.

2 Material and methods

2.1 Adaptation of the PBPK model for pregnancy

2.1.1 Pregnancy and fetal compartments

The pregnancy PBPK model (p-PBPK) for Pb was based on the model developed by O'Flaherty [20, 48-51]. In this paper, the parameterization described in [20] was used. Briefly, the O'Flaherty's model simulates the Pb disposition from birth to adulthood following inhalation and ingestion. The model includes seven compartments, including cortical bone, trabecular bone, liver, kidneys, blood, poorly-perfused and well-perfused tissues. Pb is distributed to the organs by the plasma: the levels in the organs are driven by tissue:plasma partition coefficients and limited by blood flows. Excretion occurs in kidney and liver via urine and bile, respectively. Total excretion is modeled as a function of the glomerular filtration rate (GFR). The structure of the bone compartments and the exchanges that govern them are central in this PBPK model. The model makes a distinction between cortical and trabecular bones [50]. Cortical and trabecular bones are divided into mature and juvenile bones. Pb uptake is modeled in cortical and trabecular bones and Pb elimination from bones is based on physiological mechanisms such as osteoporosis in the case of normal bone loss in human aging and remodeling of the mature bone. In childhood, simultaneous bone resorption and formation result in a net increase of bone mass, whereas in young adults there is no change in bone mass. The rates of bone formation and resorption are age-dependent. Some physiological parameters of the PBPK model depend on age (*i.e.*, the absorbed fraction of Pb in the gastrointestinal tract, hematocrit and total clearance from plasma) or body weight (*i.e.,* respiration rate, glomerular filtration rate, cardiac output, blood flows, organ volumes, bone volume, bone mass and bone density).

The p-PBPK model for Pb (Figure 1) was developed by adapting the O'Flaherty model to the pregnant woman and her fetus. The adipose tissues and mammary glands compartments were added to the maternal sub-model. The fetal sub-model includes the same compartments as the maternal one without the mammary glands. A brain compartment was included in both the maternal and fetus models because of Pb effects in fetal brain development and to ensure consistency between the maternal and fetal sub-models. The placenta

forms a complex and dynamic interface between the fetus and the mother and governs the feto-maternal exchanges [52]. The placenta is formed by an inner cytotrophoblast layer and an outer multinucleated syncytiotrophoblast layer. The Pb exchanges between the maternal and fetal sides of the placenta were modeled by diffusion [53-55]; these exchanges are the only routes of uptake and elimination of Pb by the fetus. A bidirectional transfer constant between the maternal and fetal placentae was assumed. As proposed by Codaccioni *et al.* [42, 43, 56], the rate of placental diffusion (RD_{pl}) was scaled to the placental membrane exchange surface and to the thickness of syncytiotrophoblast, inducing an increase in placental transfers during pregnancy:

$$RD_{pl} = KD_{pl} \times CBP\_PL \times \frac{T_{sct}(t)}{T_{sct}} \times S_{sct}(t) \qquad \textit{(Eq. 1)}$$

Where KD_{pl} is the constant of diffusion between both placentae during pregnancy (in L.day^{-1}.dm^{-2}), RD_{pl} is the rate of diffusion in the placenta in mg.day^{-1}, CBP_PL is the concentration of Pb in blood plasma in the placenta (maternal of fetal) µg.L^{-1}, $S_{sct}(t)$ (in dm²) is the placental exchange surface as a function of fetal age (*FA*), T_{sct} is the syncytiotrophoblast thickness at the end of pregnancy (0.00009 dm) and $T_{sct}(t)$ is the thickness according to fetal age (in dm) (see the equations in Table S1 in supplementary data).

2.1.2 Parametrization of the p-PBPK model

Several maternal parameters were modified to incorporate their evolution during pregnancy. Changes in hematocrit, glomerular filtration rate, cardiac output, blood flows and compartment volumes were modeled as functions of the gestational age (*GA*), fetal age (*FA*), or bodyweight [57-59] (see Table S1 in supplementary data). *FA* denotes the elapsed time since the ovum fertilization whereas GA considers the time since the first day of the last menstrual period that precedes conception. Ovum fertilization occurs, on average, 2 weeks after the last menstrual period.

In the fetus, the cardiac output and the relative blood flow to the brain, kidneys, ductus venosus, portal vein and umbilical cord were modeled as proposed by Abduljalil *et al.* [59]. The blood flow in the hepatic sinus was calculated as the difference between the flow through the umbilical cord and ductus venosus. The fraction of

umbilical cord blood flow attributed to the ductus venosus decreases with the progression of pregnancy which increases the blood supply to the liver by the hepatic sinus. The liver blood flow was calculated as the sum of the hepatic artery and portal vein blood flows. Changes in fetal hematocrit were modeled as described by Zhang *et al.* [60]. All equations related to the blood flows in fetus and hematocrit are reported in Table S2 in supplementary data. Excretion to and uptake from the meconium were assumed to be non-significant [61] and were not modeled.

The fetus's body weight (BW_f in grams) was modeled using the following Gompertz equation [62]:

$$BW_f = 0.00137 \times exp\left(\frac{0.1974}{0.01306} \times [1 - exp(-0.01306 \times FA)]\right) \quad \textit{(Eq. 2)}$$

where FA is the fetal age in weeks.

Fractional weights of fetal organs were either constant or modeled as a function of age. The values of mass of organs or tissues in newborns were set to the values reported by the ICRP [63] and were used to calculate the relative weights of bone, mammary glands, bone marrow, sexual organs, skin, urinary tract, gut, stomach and non-perfused bone (See Table S3 in supplementary data). The relative weights of adrenals, brain, heart, skeletal muscle, pancreas, spleen, thyroid, kidneys, lung and liver were calculated as a function of the age of the pregnancy [39] (See equation in supplementary data, section Volume of fetal organs). The relative weight of adipose tissue was calculated as the difference between total weight of other perfused and non-perfused organs, and bodyweight. The density of organs in the fetus was assumed to be equal to 1 except for adipose tissue and bones. The density of adipose tissue was set to 0.9 [64]. The density of bone tissue in the fetus was modelled as increasing from 1.3 at the start of ossification to 1.8 by extrapolating the equation in the O'Flaherty model [20]. The modeling of bone growth in the fetus is discussed further in section 2.1.3. The density of bone tissue increased from 1.8 at birth to 1.9 in adulthood as modeled in the O'Flaherty model [20].

Substance-specific parameters were set based on values used by O'Flaherty [20]. Tissue:plasma partition coefficients for adipose tissue and mammary glands were set to the value for poorly-perfused tissues given in the O'Flaherty model (See Table S4 in supplementary data). The brain:plasma and placenta:plasma partition

coefficients were set to that of well-perfused tissues. The fetal tissue:plasma partition coefficients were assumed to be equal to the maternal values. The fractional clearance of Pb from plasma into new bone in the fetus was set to that of the mother (15,000 L of plasma cleared per L of bone formed).

2.1.3 Modeling of bone growth in the fetus

Bone growth during fetal life was described according to several assumptions. Firstly, the proportions of cortical and trabecular bone volumes and blood flows were assumed to be the same as in the maternal PBPK model. The main difference compared to the maternal model is that all bone was assumed to be immature in the fetus over the whole pregnancy. Before 13 weeks of *FA*, the bone compartment was assumed to be cartilage and no Pb accumulation occurs. Between 13 and 26 weeks of *FA*, the relative volumes of cortical and trabecular bone increased linearly up to the values at birth. After 26 weeks, the relative bone volumes remain constant. When the ossification starts (*i.e.,* after 13 weeks of *FA*), Pb deposition into bone was modeled as in the maternal PBPK model, that is a function of Pb clearance from plasma into forming bone, the rate of bone remodeling and the concentration of Pb in plasma (See the structure of bone compartments in adult and fetus Figure S1 in supplementary data).

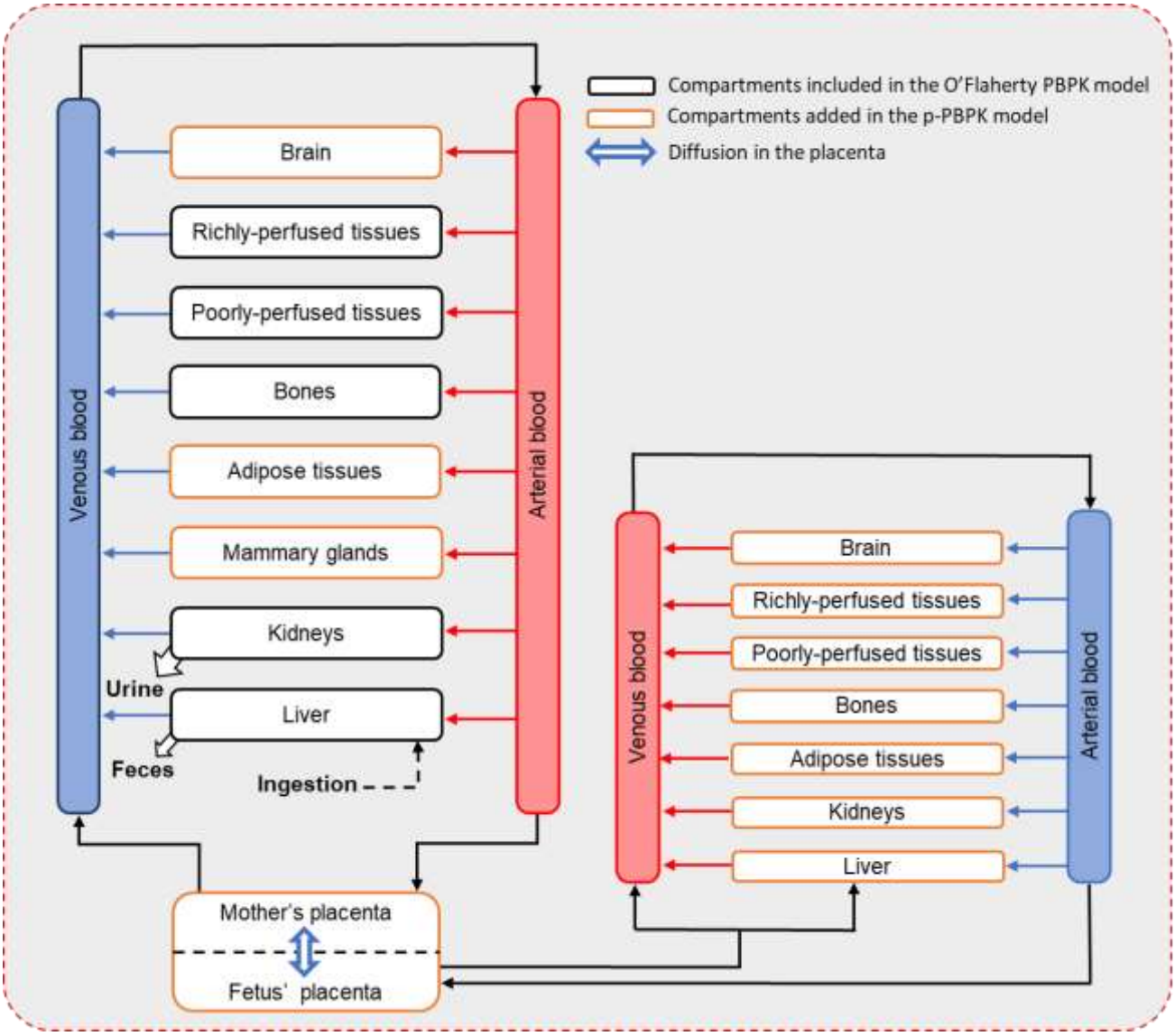

Figure 1: Structure of the p-PBPK model for Pb. The mother's exposure is by ingestion and the fetus' exposure is mediated by simple diffusion of Pb across the placenta. The Pb is eliminated through urine and bile in the mother.

2.1.4 Additional maternal bone remodeling during pregnancy

Data quantifying the maternal bone remodeling during pregnancy is limited. Biochemical markers such as free pyridinoline (fPyr), free deoxypyridinoline (fDPyr) and N-telopeptide (NTx) can be used to assess bone resorption as they are the degradation products of type I collagen. For instance, they are used to assess osteoporosis, fracture risk and other bone diseases. Two studies have shown that bone resorption increases during the 2nd and 3rd trimesters of pregnancy [65, 66]. Increase of markers of formation, bone-specific alkaline phosphate (BSAP) and procollagen extension peptide (P1CP) were also observed at the 3rd trimester. We then included in our p-PBPK model the increase of bone remodeling during pregnancy and it was modeled by additional formation and resorption, under the assumption of constant bone volume and weight [67]. The

following equations were used to compute the additional bone turnover (*BRRP* unitless) and rate of formation of bone (*BFR* in L.day^{-1}) in the mother:

$$if\ FA < STBR \qquad BRRP = 0.0$$

$$if\ FA \geq STBR \qquad BRRP = CABR \times (FA - STBR) \qquad \textit{(Eq. 3)}$$

$$BFR = FBFR \times VBONE \times (1 + BRRP) \qquad \textit{(Eq. 4)}$$

Where $CABR$ is the coefficient representing the magnitude of additional remodeling (week^{-1}), *STBR* is the age of the fetus (in weeks) at which addition remodeling starts, *FBFR* is the fraction bone formation rate (day^{-1}), *VBONE* is the bone volume (L).

2.2 Model calibration

The parameters for additional bone remodeling and placental diffusion were estimated by Bayesian inference using, respectively, maternal BLLs over pregnancy and paired concentration data in the mothers and newborns at delivery. Rothenberg's study [25] was used to estimate additional bone remodeling (parameters *CABR* and *STBR*). In their study, Pb in maternal blood was measured in 105 women living in the valley of Mexico between March 1987 and June 1992. Samples were taken from week 12 to week 36 of pregnancy. Among these women, the mean gestational age was 39.9 weeks, and the mean maternal age was 27.5 years. Data from a separate study [68] was included to calibrate the diffusion constant of Pb in the placenta (KD_{pl}). This study reported Pb levels in the mother's blood and cord blood at delivery in 47 mother-newborn pairs [68]. The gestational age and the mother's age were not reported: for our simulations, we assumed a mean age of women of 29 and a gestational age of 39 weeks at delivery.

From these two datasets, the parameters $CABR$ and $STBR$ were estimated as population parameters; KD_{pl} and the interindividual variability of KD_{pl} were estimated in a hierarchical model which produced an estimate of KD_{pl} for each woman. Because the exposure of the women was not known, the daily intake (*DI*) of each woman was also estimated independently for each woman assuming a constant exposure per unit body weight of the women since the birth. The p-PBPK model was calibrated using a Bayesian approach with Markov Chain

Monte Carlo (MCMC) simulations using the Metropolis-Hastings algorithm. A non-informative uniform *prior* distribution between 0 and 30 was assigned to the magnitude of additional bone remodeling, $CABR$. According to Black *et al.* study [65], markers of bone resorption (*i.e.,* fPyr, fDPyr and NTx) were significantly increased from 14 weeks of gestation (p-value < 0.02). As a result, a truncated normal *prior* distribution around 14 weeks with a coefficient of variation of 50% was assigned to $STBR$ and truncated between 12 and 29 weeks of *FA*. A populational model was used to account for the interindividual variability of placenta transfers. The individual placental transfers were lognormally distributed around a population mean and a population standard deviation. The *prior* distributions of the population mean, KD_{pl} and the geometric standard deviation, SD_KD_{pl}, were log-normal distributions truncated between 10^{-4} and 0.5 $L.day^{-1}.dm^{-2}$ and between 1 and 5, respectively. The *DI* was estimated for each mother. A *prior* uniform distribution between 0.1 and 100 $\mu g.day^{-1}.kg^{-1}$ was assigned. Three independent MCMC chains were launched with 60,000 iterations each. Results are based on the last 10,000 iterations. The Gelman's index, $\hat{R}$, was used to assess convergence that was assumed to be achieved when $\hat{R}$ was smaller than 1.1.

2.3 Evaluation of the p-PBPK model for Pb

2.3.1 Sensitivity analysis

A sensitivity analysis (SA) using the Morris method [69] was conducted as a preliminary screening to identify the most influential parameters on the venous concentrations in the mother and fetus, the cord blood:mother blood ratio, and the concentration in the fetus' brain at the end of each trimester of pregnancy (*i.e.*, 13, 26 and 39 weeks). The SA was run for a woman with pregnancy at 27.5 years and constantly exposed to 2 $\mu g.day^{-1}.kg^{-1}$ of Pb. Exposure was started at age 10 to reach a steady state in plasma before the pregnancy. A total of 71 input parameters were selected for this first step (See Table S5 in supplementary data). A uniform distribution of ±5% around the mean values was assigned for all parameters. The parameters with the highest impact on the model outputs were selected for a second step of SA using the Sobol method [70, 71]. The method decomposes the variance of the model outputs into sums of variances of the input parameters. A

uniform distribution of ±10% was assigned to the value of parameters. First- and total-order sensitivity indices, named FOI and TOI respectively, were calculated.

2.3.2 Uncertainty and variability analysis

Variability and uncertainty of fourteen influent parameters was considered in Monte Carlo simulations, except for the parameters of Pb binding to red blood cells, to provide prediction intervals for model outputs. Model parameters selected after SA were randomly sampled as reported Table S6 in supplementary data for a woman with pregnancy starting at 29 years old and constantly exposed to 3.9 µg.day^{-1}.kg^{-1} of Pb per day since birth. Gestation duration was set to 39 weeks. The distributions of $CABR$, $STBR$ and KD_{pl} parameters were based on the *posterior* distributions obtained by model calibration.

2.3.3 Comparison with literature data

The p-PBPK model for Pb was evaluated using observed ratios between Pb levels in the umbilical cord and maternal blood in five studies [21, 72-75]. Their characteristics are reported in Table 1. Blood samples were collected at delivery or within hours. Mean gestational age was reported in one study [74], otherwise, it was set to 39 weeks.

Table 1: Characteristics of the paired data of umbilical cord and maternal blood used to evaluate the p-PBPK model. Data was collected at delivery.

Reference	Sample size	Gestation age	Country	Date
Ong *et al.* [72]	97	39 weeks *	Malaysia	From February 1983 to May 1984
Yazbeck *et al.* [73]	15	39 weeks *	France	From December 2003 to Mai 2004
Gulson *et al.* [21]	33	39 weeks *	Australia	1997
Ladele *et al.* [74]	269	38.2 ±5.2 weeks	Nigeria	From August 2014 to August 2016
Alemam *et al.* [75]	158	39 weeks *	Libya	From January 2014 to May 2015

*Set to 39 weeks

2.4 Software

The p-PBPK model (DOI: 10.5281/zenodo.8032483) was developed in GNU MCSim [76, 77] version v6.2.0. Graphical representations were made using R version 4.2.2 [78]. Data of bone turnover markers and some BLLs were extracted from plots in the original publications with Plot Digitizer free software, version 2.6.9 - 9 October 2020 [79].

3 Results

3.1 Model calibration

3.1.1 Estimation of the model parameters

The values of the convergence criterion $\hat{R}$ for the 3 MCMC chains were below 1.1 indicating that convergence was reached for all parameters. Two mother-newborn pairs of the study of Nashashibi *et al.* [68] were excluded because the MCMC chains were not able to converge, probably due to high values of the observed ratio of the cord blood over the maternal blood concentration (1.90 and 2.04). The *posterior* distributions of the estimated parameters are reported in Table 2. The mean *DI* of the mothers from the Rothenberg's study were estimated to 1.9 (± 0.034) µg.day^{-1}.kg^{-1} and 4.0 (± 1.2) µg.day^{-1}.kg^{-1} from the Nashashibi's study. Regarding the placental transfers, the estimated KD_{pl} were highly variable between the mother-newborn pairs, as shown by the high value of the population standard deviation SD_KD_{pl}. The rates of diffusion in the placenta were all estimated between 4.6 and 283 L.day^{-1} at the end of pregnancy. The population distribution of KD_{pl} is represented in Figure 2 as a boxplot by sampling in the lognormal distribution defined by the estimated population mean $KD_{pl}$and the estimated standard deviation of KD_{pl} (estimates reported in Table 2); Figure 2 also represents the individual $KD_{pl}$of the 45 mother-newborn pairs as dots on top of the boxplot. The distribution of individual KD_{pl} appears to be uniform within a wide range (min=0.005 and max=0.311 L.day^{-1}.dm^{-2}) in contrast to the population distribution which has wider bounds (Figure 2). A positive correlation was observed between *CABR* and *STBR* indicating that the later the onset of additional bone remodeling, the higher the estimated magnitude of remodeling. A negative correlation was observed between the *posterior* distributions of *CABR* and *DI* which indicates that, in the model outputs, higher additional bone remodeling is compensated by lower individual daily intakes. There is no relationship between the diffusion constant in the placenta and additional bone remodeling parameters. All Spearman correlation coefficients are available in supplementary data (Figure S2).

Table 2: Specification of prior distributions and posterior values after calibrations.

Parameter name	Abbreviation	Unit	*Prior* distribution	*Posterior* distribution		
				MPV [b]	Median	95% CI [c]
Coefficient of additional bone remodeling	$CABR$	Unitless	*Uniform [0, 30]* [a]	0.532	0.763	0.379 – 1.36
Start time of additional bone remodeling	$STBR$	Week of pregnancy	*NormalT [14, 7, 12, 29]* [a]	19.4	20.6	17.6 – 23.4
Constant of placental diffusion	KD_{pl}	L.day^{-1}.dm^{-2}	*LogNormal [10^{-4}, 0.5]* [a]	0.0531	0.0430	0.0287 – 0.0874
Variability of KD_{pl}	SD_KD_{pl}	L.day^{-1}.dm^{-2}	*Uniform [1, 5]* [a]	3.18	2.89	1.99 – 4.69

[a] Uniform and Log uniform distribution [lowest bound, highest bound], Truncated normal distribution [mean *prior*, coefficient of variation, lowest bound, highest bound].

[b] MPV stands for the Most Probable Value represented by the maximum likelihood.

[c] 95% credibility interval.

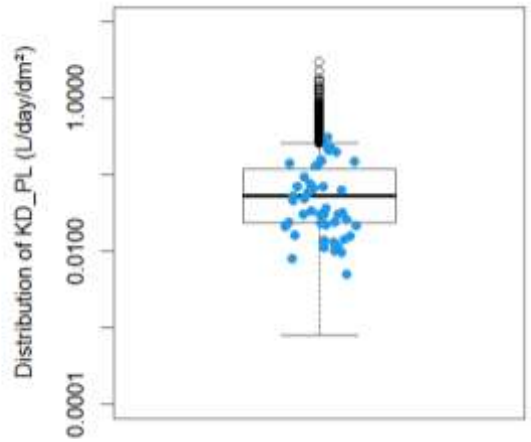

Figure 2: Boxplot of the lognormal distribution of the placenta transfer using the estimated MPV of KD_{pl} (population mean and standard deviation). 3000 simulations were run. The blue dots represent the 45 KD_{pl} values estimated during MCMC calibration.

3.1.2 Model fit to the calibration data

The estimated maternal BLLs and the 95% credibility interval (CI) during pregnancy are presented in Figure 3 with the data used for model calibration [25]. All mean observations but one are encompassed in the 95% CI. Estimated variability is slightly lower than measured variability represented as the standard error of the mean (SEM). This can be explained by the fact that the model was calibrated with the mean data only, meaning that no variability between women was accounted for. For instance, the same exposure was estimated for all

women. The median predicted maternal BLL decreased by 32% between the beginning of pregnancy and the start of additional bone remodeling (21 weeks of fetal age), mainly due to the hemodilution and the increase of the maternal volume of distribution. Between the beginning of the additional bone remodeling and the end of pregnancy, the predicted median BLL is increased by 19% because of Pb bone release into maternal blood.

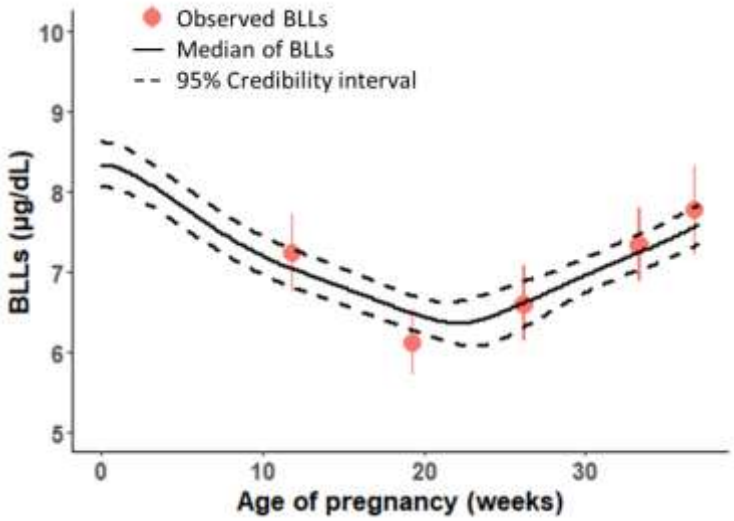

Figure 3: BLLs following constant exposure in pregnant women. The dashed curve represents the 95% credibility interval of BLLs. The solid line represent the median of BLLs. The red dots represent BLLs (geometric mean and SEM) of pregnant women measured in the Rothenberg et al. study [25].

Figure 4A presents the goodness-of-fit graph for the Pb concentrations of the mother-newborn pairs [68]. Most concentrations in the mother and fetus were predicted within a 1.1-fold error range (84%), and all BLLs were predicted within a 2-fold error range, indicating a good agreement with the observations. Figure 4B presents the cord blood:mother blood ratios. All predicted ratios were below 1.1, even for the pairs with an observed ratio above that value (*i.e.*, observed ratios reach 1.14, 1.17, 1.19 1.29 and 1.47). 98% of ratios were predicted in 2-fold error range versus 22% in 1.1-fold error range. The median predicted cord blood:mother BLL ratio was 0.88.

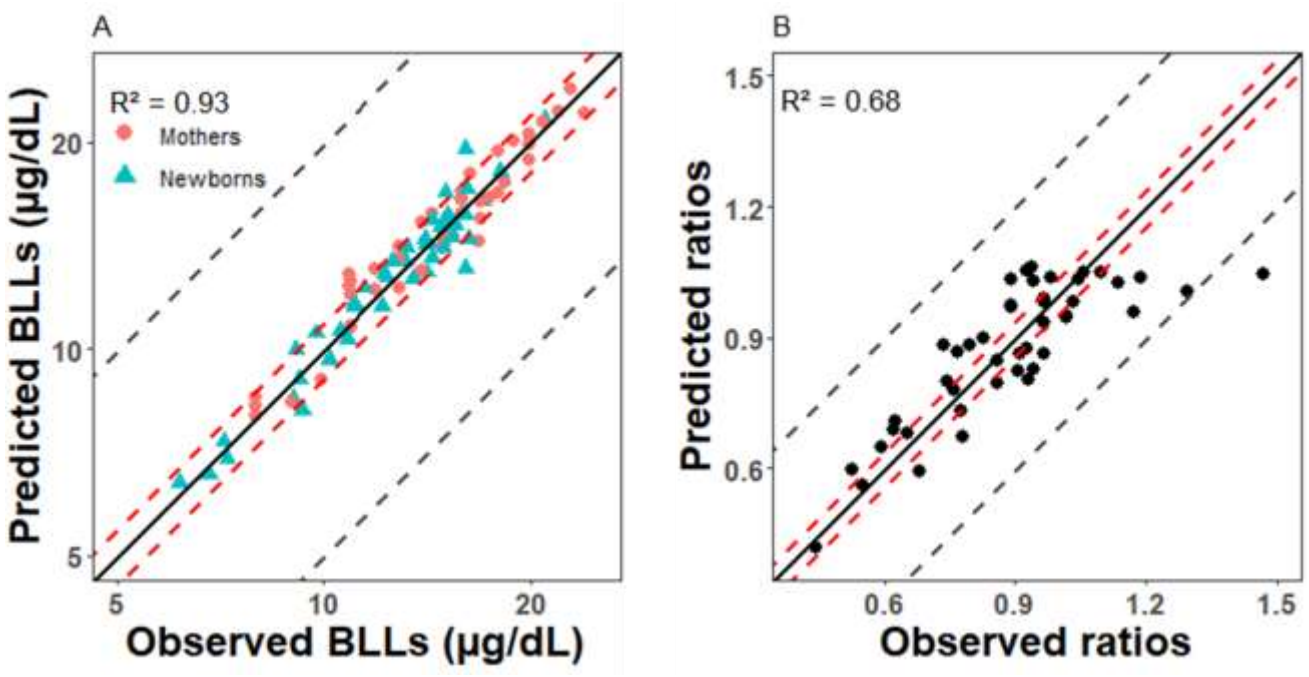

Figure 4: p-PBPK model calibration results for 45 mother-newborn pairs [68]: A) Predicted vs. observed BLLs at delivery in maternal blood and umbilical cord blood, logarithmic scale. B) Observed versus predicted ratios between umbilical and maternal venous BLLs at delivery and interval of predictions. The black solid lines represent x=y and the dashed lines represent a 1.1 (red) or 2 -fold error (grey) respectively.

3.2 Influence of model parameters on Pb kinetics

The 10 most influential parameters were selected after SA using the Morris method for each model output at the 3 trimesters of pregnancy which resulted in the selection of a total of 25 parameters for the global sensitivity analysis. The sensitivity of the blood concentrations in fetal brain (target organ) and the cord blood:mother ratio at the end of each trimester of pregnancy to the selected model parameters are represented in Figure 5. The SA of BLLs in fetus and mother are available in supplementary data (Figure S2). Parameters related to Pb binding to red blood cells (*i.e.*, *BIND* and *KBIND*) had an impact on Pb concentration in maternal blood (results shown in Figure S2) and cord blood:mother blood ratio all along pregnancy. The accumulation in maternal bones (*i.e.*, *VEXPO* and *WEXPO*) had an impact on Pb concentrations in maternal and fetal blood during pregnancy (results are shown in Figure S2 in supplementary data). All four model outputs are sensitive to the onset of additional bone remodeling, *STBR*, in the 2nd trimester which results in increased internal Pb exposure. Pb binding to fetal red blood cells (*BINDF* and *KBINDF*) impacts the BLLs in fetus and the cord blood:mother blood ratio but does not affect fetal Pb levels in brain at the 3 trimesters of pregnancy due to distribution by plasma. Fetal bone parameters (*VEXPOF*, *WEXPOF* and *RCORF*) impact the

fetal Pb blood and brain concentrations at the 2nd and 3rd trimester when the formation of bone tissue begins in fetus. Pb is then stored in the fetal bones. Other mechanisms such as the transfer of Pb across the placenta (KD_{pl} and *T_sctR*) influence the fetal concentration of Pb during the 2nd and 3rd trimesters. Pb in the fetal brain is sensitive to the partition coefficient in the brain (*pInv_BRF*) and to the Pb burden in maternal and fetal bones (*VEXPO*, *WEXPO*, *VEXPOF* and *WEXPOF*). However, the model's outputs are relatively insensitive to the parameters listed in Table 2 (KD_{pl}, *STBR, CABR*). This could explain the large uncertainty and variability on KD_{pl} and *CABR* represented in the *posterior* distributions and means that the mother-newborn data do not contribute greatly to the estimation of *STBR* which was influent only during the 2nd trimester. There was no difference between the FOI and TOI sensitivity indices.

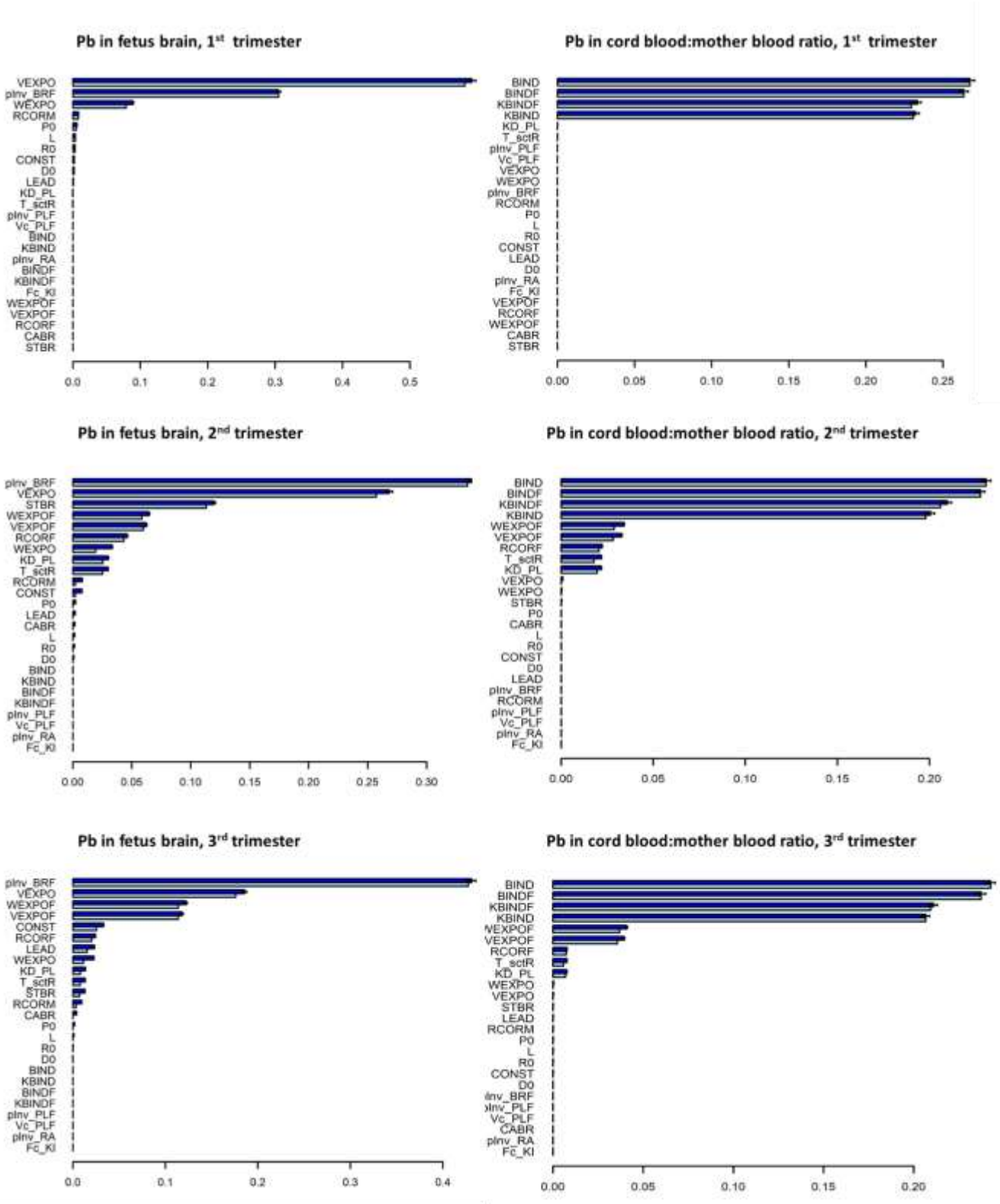

Figure 5: FOI (light blue) and TOI (blue) from the Sobol sensitivity analysis: Pb Levels in the fetus brain and cord blood:mother blood ratio at the 1st, 2nd and 3rd trimesters of pregnancy.

3.3 Evaluation of the calibrated model

Results from 3,000 MC simulations for women with a beginning of pregnancy at age 29 and a gestation duration of 39 weeks are presented in Figure 6A and Figure 7. The exposure dose of 3.9 µg.day^{-1}.kg^{-1} corresponded to the average dose of the women included in the Nashashibi *et al.* study [68]. The predicted ratios of cord blood:maternal blood at delivery were 0.92 and 0.88 after exposure to a dose of 0.39 µg.day^{-1}.kg^{-1} and 39 µg.day^{-1}.kg^{-1} respectively. Figure 6 shows the median of the cord blood:mother blood ratio throughout pregnancy with the 95% of CI (Figure 6A), as well as the distribution of the observed ratios reported in five studies (Figure 6B) [21, 72-75]. The median ratio was estimated to be 1 at the end of pregnancy according to the p-PBPK model. The median values for Alemam *et al.* [75], Gulson *et al.* [21], Ladele *et al.* [74], Ong *et al.* [72], and Yazbec *et al.* [73] were observed to be 0.79, 0.82, 0.82, 0.81, and 0.98, respectively. In the study of Ladele *et al.* [74], ratios were highly variable compared to our credibility interval. In their paper, the authors reported that 18% of the samples had higher BLLs in the cord than in the mother resulting in ratios greater than 1. 29% of the cord blood:mother blood ratios were greater than 1, for all studies combined , which is not the case with our current p-PBPK model predictions.

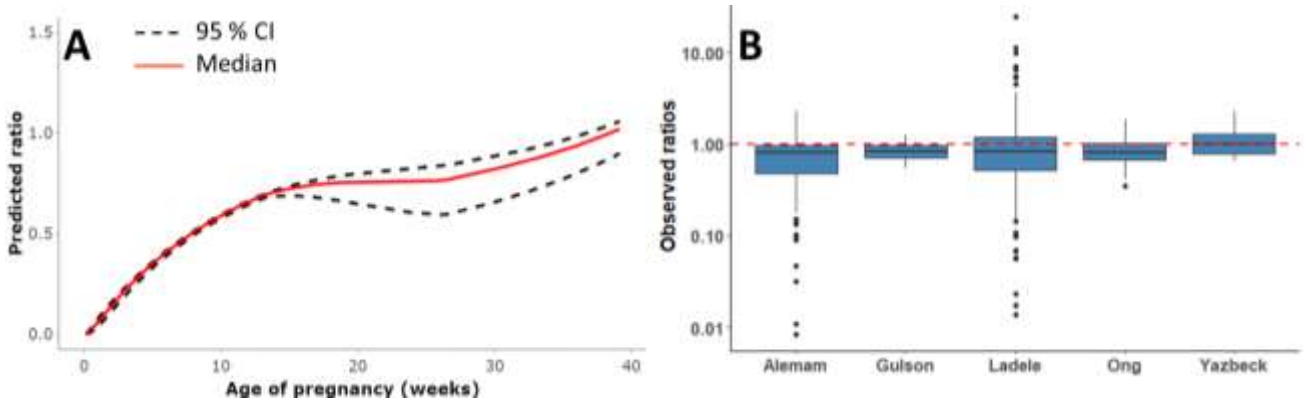

Figure 6: Predicted cord blood:mother blood ratios during pregnancy and observed ratios at delivery. A) The solid red curve represents the median of predicted ratios, and the black dashed curves represent the 95% CI of predicted ratios by the p-PBPK model for 3,000 MC simulations. B) The boxplots represent the distribution of ratios computed with measured concentrations reported in five studies [21, 72-75] and the dashed line the predicted ratio at delivery by our p-PBPK model.

The results of MC simulations on bone formation rate, Pb concentrations in fetal bones, blood and brain are presented in Figure 7. The bone formation rate in the fetus is set to zero until the end of the 1st trimester (13 weeks of *FA*) and then varies as pregnancy progresses (Figure 7A). During the 3rd trimester, the rate of bone formation decreases: the ratio between the rate of change of bone volume and the fetal body weight

decreases while bone Pb levels continue to increase. The kinetics of Pb in fetal bones (Figure 7B), blood (Figure 7C) and organs such as brain (Figure 7D) are different but characterized by three phases hence the importance of modelling them. This difference in the kinetic profile of Pb levels in blood and other organs (*e.g.,* brain) can be explained by the fact that fetal hematocrit is very low at the start of pregnancy and that Pb levels in organs reflect the plasma kinetics rather than the blood kinetics. The first phase is due to the small volumes of fetus and the absence of bone tissues resulting to high Pb concentrations in fetal blood and brain. At the beginning of the 2nd trimester, cartilage turns into bone tissue which allows the incorporation of Pb and thus the decrease of BLLs in the fetus since the bone formation drags Pb out of the plasma faster than the rate of incoming Pb by placental transfer. The onset of additional maternal bone remodeling around week 20 leads to Pb release in maternal blood and an increase in fetal exposure during the 3rd trimester.

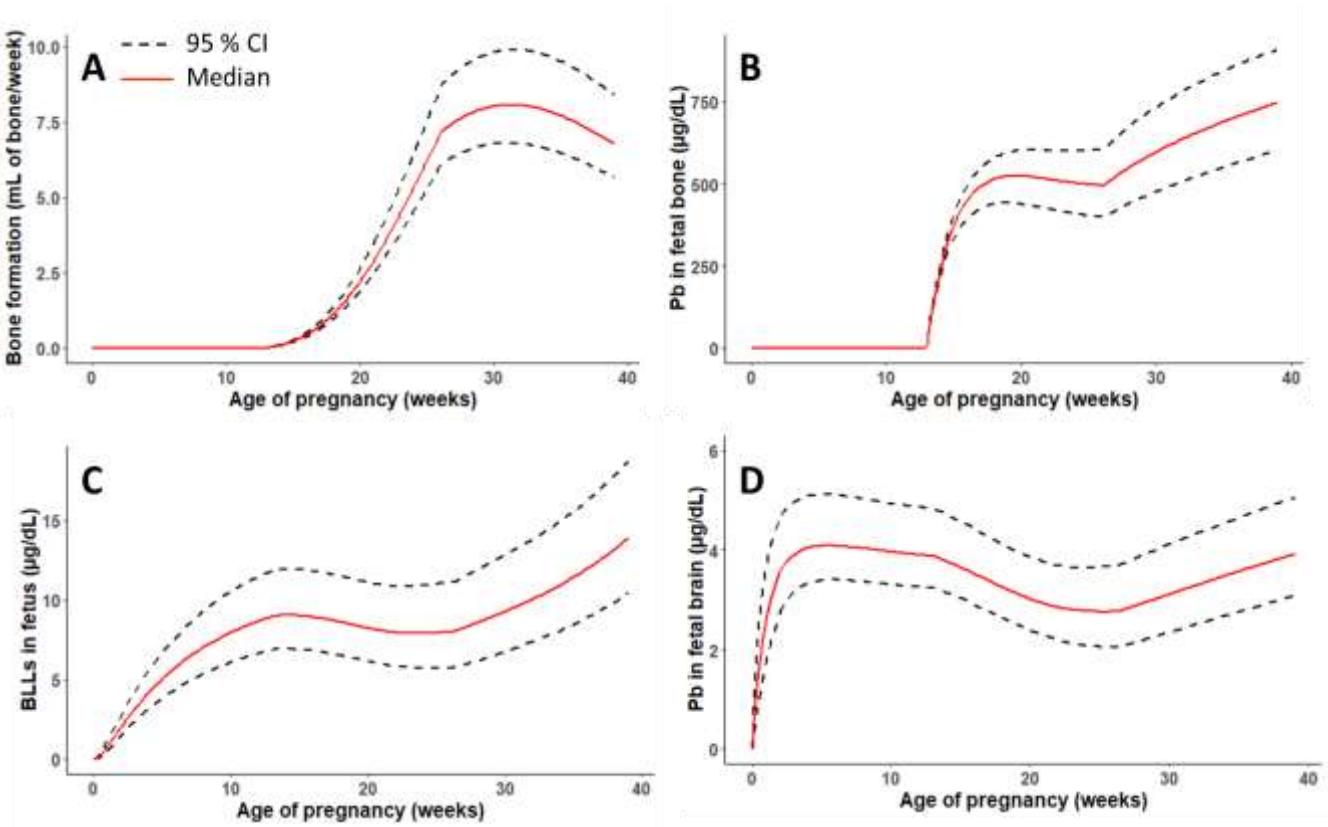

Figure 7: Kinetics predicted using Monte Carlo simulations and the p-PBPK model for women constantly exposed to 3.9 $\mu g.day^{-1}.kg^{-1}$ *of Pb per day since birth. 95% of IC were calculated on a random sample of 3,000 simulations: A) bone formation rate of in the fetus, B) Pb concentrations in the fetal bones, C) in the fetal blood and D) in the fetal brain.*

4 Discussion

A p-PBPK model was developed to predict the kinetics of Pb in pregnant women and their fetuses throughout pregnancy. The O'Flaherty model developed for children and adults was extended to incorporate maternal physiological and anatomical changes, and fetus growth during pregnancy. The structure of the p-PBPK model integrates different compartments and physiological mechanisms such as additional bone remodeling to describe fetus exposure through feto-maternal exchanges via the placenta. The bone compartment in the fetus was modeled to incorporate Pb as soon as bone tissue appears.

The present p-PBPK model includes the distribution of Pb in cortical and trabecular bones in the mother and fetus. The metal is primarily distributed to the metabolically active bone region in the mother and diffuses into the deeper layers [51]. Additional bone remodeling was implemented in the maternal model to describe Pb release from bone to maternal blood during pregnancy. This release is mainly explained by the physiological maternal adaptation regarding calcium metabolism to meet the fetus needs. The sensitivity analysis shows that both maternal and fetal kinetics are sensitive to the bone Pb burden accumulated over time and to the time of onset of additional bone remodeling. As a consequence, the maternal BLLs simulated with our model show a characteristic U-shape curve as observed in several studies [26, 27, 80]. Our model predicts an increase of 23% in maternal BLL between the start of additional bone remodeling and the end of pregnancy. The predicted increase is similar to observations. For instance, In the Ettinger *et al.*'s study [27], the BLL value reported at 6 months of pregnancy was 22% higher than the value reported at 8 months. In the study by Hu *et al.* [26], the value of BLL at delivery was 19% higher than the one measured during the 2nd trimester.

The Pb kinetics in the fetus evolve during pregnancy due to variations in the maternal internal exposure, to fetus growth especially ossification, and to the Pb placental transfers that depend on the placental physiology. Fetal kinetics are characterized by a peak in blood levels at the end of the 1st trimester followed by a slight decrease until the end of the 2nd trimester, and then by an increase until the end of pregnancy. Several p-PBPK models have been developed for predicting the fetal kinetics throughout pregnancy for environmental contaminants. In their study, Gentry *et al.* [81] predicted the fetal kinetics of six compounds (isopropanol, vinyl chloride, methylene

chloride, perchloroethylene, nicotine, and TCDD) and showed that the characteristics of compounds influence the fetal kinetics [81]. In the fetus, the levels of isopropanol and its metabolite (acetone) were influenced by the levels in the mother's bloodstream. Toward the end of the 1st trimester, fetal levels of isopropanol sharply decreased because of fetal alcohol dehydrogenase metabolism. However, acetone came from the mother's bloodstream because the enzyme CYP2HE1 responsible for the metabolism of isopropanol was not present during prenatal life. The blood levels of vinyl chloride and methylene chloride remain relatively constant during gestation. Perchloroethylene, nicotine, and TCDD present a concentration peak at the start of the pregnancy and remain relatively constant because of changes in tissue composition in the mother and fetus during pregnancy. In summary, all these factors contribute to the complexity of chemical exposure during the gestation period.

While our p-PBPK model is a valuable tool for simulating fetal exposure, it is essential to acknowledge its limitations and uncertainties when interpreting its predictions for risk assessment purposes. Assessing the predictability of a p-PBPK model is a difficult task because there is only a small amount of data available about fetal toxicokinetics to build and verify such models [82, 83]. The p-PBPK model for Pb was evaluated using the ratios between Pb levels in the umbilical cord and maternal blood at delivery, as usually done for p-PBPK models [43]. However, for obvious ethical reasons, it would not be possible to acquire such data at other times of the pregnancy. To overcome the limitation of evaluating the p-PBPK model on time-course concentration data, it is necessary to provide confidence in parameter values used for describing the ADME processes. Regarding the biological plausibility, the most up to date studies were used for assigning the physiological and anatomical parameter values of the fetus [57, 59, 63, 84]. Further research and data collection could help in refining other parameters that highly influence the blood levels and the Pb concentrations in target tissues. Adult values were assigned for several of these parameters, as binding parameters in blood (*BIND* and *KBIND*), accumulation in bones (*LEAD*) or tissue's affinity. For that latter, a way to refine their values could be to dose Pb and environmental contaminants in aborted fetuses [85, 86].

Some uncertainties remain in the placental transfer rates during the early stages of pregnancy because of a lack of knowledge. To calibrate those rates, the only data available are usually the cord blood concentrations at delivery

(as in our study). Radioactive tracer studies were conducted on rodents [87] but, due to differences in the placenta's structure, extrapolation of placental transfers between animals and humans is not straightforward. The placenta grows throughout pregnancy and provides a large surface for maternal-fetal exchanges. The villi are in the intervillous space and provide contact area with maternal blood. Their number increases during pregnancy leading to a reduction of the between distance the maternal and fetal blood circulation [55, 88]. In our model, the Pb diffusion constant was linked to the placental physiology, (*i.e.,* to the thickness and the surface area of the syncytiotrophoblast). That assumption on evolving placental transfers has an influence on the Pb fetal kinetics, as shown by the results of the sensitivity analyses and by two p-PBPK models for perfluorooctanoic acid (PFOA) and perfluorooctane sulfonate (PFOS) [43, 89]. Loccisano *et al.* [89] predicted that the PFOA and PFOS concentrations in fetus blood follow the same trend as the mother's ones that decrease as the pregnancy progresses. In that model, the transfer rates were scaled to the fetal body weight. In their study, Brochot *et al.* 2019 [43] predicted an increase of fetus exposure throughout pregnancy with the placental transfer rate scaled to the placenta volume. These two studies highlight the importance of assumptions made to model the placental transfers. Using a model for the placental transfer rates based on the physiology of the placenta should lead to an improved characterization of the fetal internal exposure especially during the early months of pregnancy when no kinetic data is available.

At delivery, our p-PBPK model estimates a mean ratio of newborn BLL over mother BLL of 1.01 ± 0.04 under a constant exposure scenario, highlighting that our model is not built to predict a higher Pb accumulation in fetus' blood than in mother's blood. Indeed, Pb is assumed to be distributed to the fetus by bidirectional passive diffusion in the placenta. Several studies have measured the Pb concentration in cord blood and maternal blood. In the studies conducted by Alemam *et al.* [65], Gulson *et al.* [9], Ladele *et al.* [18], Ong *et al.* [63] and Yazbec *et al.* [64], the respective median values of cord blood:mother blood ratios were observed to be 0.79, 0.82, 0.82, 0.81, and 0.98. Among the five studies examined, approximately 71% of the pairs had ratios less than 1. Other mechanisms in placental transfer than passive diffusion, could be involved and may explain the higher Pb blood concentration of the mother compared to the cord blood concentration. For instance, active diffusion via transporters might occur. The role of the divalent metal transporter 1 (DMT1) has been demonstrated in the intestinal uptake of Pb

[90] and DMT1 is expressed in the human placenta [91]. However, to date, no evidence has been found about the transfer of Pb across the placenta by the DMT1 transporter.

The Pb concentration in the placenta evolves during pregnancy and follows the same pattern as the Pb concentration in maternal plasma. At delivery, the median placenta blood:maternal blood ratio was estimated at 1.6 with the p-PBPK model. This value is 3 times higher than the ratio calculated (0.48) in the study by Schramel *et al.* [92], in which the Pb level measured in fresh placentae (18.7 ± 7.3 $ng.g^{-1}$) was about a half of the value measured in the maternal blood (39 ± 14 $ng.g^{-1}$). In our model, the placenta:plasma partition coefficient was set to the same value as richly perfused tissues (50). This value could be refined if new data become available on the partition between the plasma and the placenta in pregnant women. However, this uncertainty in this value is expected to have a small impact on the model predictions in the mother and in the fetus since the placental transfer rates have been estimated for measured concentrations in our study.

In the p-PBPK model, intake and elimination of Pb in the fetus occur only through the placenta. Several studies have reported measured Pb concentrations in the meconium [93, 94] and the amniotic fluid [95-97]. In our p-PBPK model, the Pb elimination by meconium was assumed to be negligible and was therefore not considered. This assumption was supported by the fact that measured meconium concentrations indicated a rather limited contamination of the meconium samples. For instance, a Canadian study analyzed 396 meconium samples and reported a median of 0.022 µg of Pb per gram of meconium and a maximum concentration of 0.35 $\mu g.g^{-1}$ [94]. Comparing these values with the MC simulations presented in the Results section where a body burden of 757 ± 80 µg of Pb was estimated for a fetus of 3.3 kg under a constant realistic exposure of the mother to 3.9 $\mu g.day^{-1}.kg^{-1}$, the median measured amount in meconium (assuming a weight of 100 g) is less than 1% of the total fetal body burden. The exposures were not necessarily similar, but both were realistic and allowed a simple comparison of their magnitudes. The same rational was applied for the amniotic fluid. Siegers *et al.* [95] reported Pb levels in amniotic fluid of 24.0 ± 9.41 $ng.L^{-1}$ (*i.e.,* 0.019 ± 0.075 µg for 800 ml of amniotic fluid), and the Pb levels were reported to be lower in maternal serum than in the amniotic fluid. Other studies reported similar ranges [96, 97].

When comparing to the fetal body burden simulated in our study, the measured Pb amount in amniotic fluid corresponds to only 0 to 0.3%.

Numerous experimental and epidemiological studies have shown that Pb can induce neurodevelopmental effects and direct effects on brain [98, 99]. For instance, experimental studies provide evidence of a cellular mechanism and a molecular target of Pb leading to neurodevelopmental effects [100-102]. The mechanism is dependent on the temporal and regional emergence of critical developmental processes (*i.e.,* neurulation, neurogenesis, microglia entry, synaptogenesis, apoptosis, gliogenesis, and myelinization) [102, 103]. Evidence points to the direct interaction between Pb and the N-methyl-D-aspartate receptor (NMDAr) located in the postsynaptic cells [101, 102, 104]: these receptors play a central role in plasticity, learning, and memory. In our p-PBPK model, the brain compartment structure is quite simple and assumes an instantaneous and homogeneous Pb distribution in all the brain regions. This structure could be improved to study the Pb exposure in the central nervous system (CNS) and to account for the blood-brain barrier (BBB). That latter limits the diffusion of molecules including heavy metals through the presence of tight junctions or effluxes proteins [105] but Pb has been shown to inhibit capillary-like structure formation in i*n vitro* models of CNS, leading to increased permeability of the BBB [106]. Some mechanistic models for CNS with various structural differences are available in the literature [107-110]. In the simplest model, the CNS was summarized as plasma and brain tissues linked by uptake and efflux clearances [110]. In more complex models, the physiological structures such as the extracellular fluid, the cerebrospinal fluid (CSF), and the blood-cerebrospinal fluid barrier are integrated [107, 108]. The application of these sophisticated brain models is often limited by the absence of *in vivo* data for model calibration and validation.

Our p-PBPK model could become a useful tool for risk assessors to simulate the fetal exposure to Pb. As part of prenatal exposure assessment and the optimization of prevention strategies, the p-PBPK model can be used to evaluate the effectiveness of various prevention strategies during pregnancy on fetal Pb levels, as well as management strategies to reduce exposure in women already exposed. The use of such models can thus contribute to improved decision-making in public health and risk management for pregnant women and their fetuses. P-PBPK models can also be applied to assess the chemical risk for the fetus. Recently, two studies have

applied p-PBPK models to make the link between *in vivo* exposure and *in vitro* effect data for developmental (neuro)toxicity [111, 112]. Both studies examined the effects of prenatal exposure to pesticides (chlorpyrifos and deltamethrin) using a quantitative *in vitro-in vivo* extrapolation (QIVIVE) approach based on a p-PBPK model. Algharably *et al.*'s [111] predicted the oral maternal exposure during pregnancy corresponding to the active *in vitro* concentration in neuronal stem cells. Their results showed that the daily intake doses predicted from the *in vitro* data were several orders of magnitude higher than exposures estimated from measured chlorpyrifos concentrations in mothers, indicating an absence of risk for the neurotoxic responses captured by their *in vitro* test battery. In the second study, Maass *et al.* [112] have compared p-PBPK model predictions for deltamethrin in fetal target organs to active *in vitro* exposure related to effects on developmental neurotoxicity. Their results indicated that the deltamethrin concentrations in the human fetal brain are unlikely to reach the *in vitro* active concentrations indicating.

Beyond elucidating the fetal Pb kinetics, the p-PBPK model can help in better characterizing the relationship between the active exposure in the target tissue at a critical time window and the onset of adverse effects. El-Masri *et al.* [113] have developed an integrative and quantitative approach to assess the potential risk of chemicals on fetal development. In their approach, the p-PBPK model was used to estimate maternal exposures that produced fetal blood levels equivalent to the chemical concentrations that altered the activity of toxicity tests linked to the most sensitive adverse outcome pathway (AOP) for vasculogenesis and angiogenesis in fetus. Predicted maternal exposures were compared with potential exposure levels, using literature data or exposure models, to derive AOP-based margins of exposures. Coupling of the p-PBPK/AOP model enabled to determine whether maternal exposure levels to chemicals were likely to induce effects such as those observed *in vitro*, considering the critical developmental stages linked to fetal vasculargenesis and angiogenesis. An extension of our work could be to couple the p-PBPK model to dose-effect relationships (as quantitative AOP) to develop a predictive model of the Pb effects on the child neurodevelopmental system during early life. There are several qualitative AOPs related to brain development, including AOP 13 from AOP Wiki, which describes the chronic binding of an antagonist to NMDA receptors during synapse formation [114]. Inhibition of these receptors triggers

a sequence of key events that lead to the emergence of adverse effects, as described in AOP 13, such as learning and memory deficits.

5 Conclusion

We presented a p-PBPK model to describe the disposition of Pb in a pregnant woman and her fetus. The model integrates pregnancy-related physiological changes such as additional bone remodeling, glomerular filtration, cardiac output, and the increase in volumes and blood flows. The time-dependent profile of Pb predicted by the model in the mother is consistent with literature data. Furthermore, Pb levels in maternal and fetal blood at delivery are well predicted. The p-PBPK model proposed here can be used to assess prenatal Pb exposure. Model predictions showed that internal exposure of the fetal organs vary during the fetus development, with a peak of exposure at the end of the 1st trimester and another peak at delivery. To our best knowledge, this is the first time that a p-PBPK model integrates bone compartments in a fetal model and offers new opportunities to describe the kinetics of compounds that are likely to accumulate in bones.

Acknowledgments

This study was financially supported by the European Union co-funded project European Partnership for the Assessment of Risks from Chemicals (PARC) under Grant Agreement No 1010570 and by the French Ministry in charge of Ecology within Programme 190.

Supplementary Information

The supplementary information is available.

The model code is available with an example simulation file at https://doi.org/10.5281/zenodo.8032483.

Declaration

The authors declare no conflict of interest.

Bibliography

1. ATSDR, *Toxicological Profile for Lead.* U.S. Department of Health and Human Services ; Division of Toxicology and Human Health Sciences ; Environmental Medicine Branch, 2020.
2. WHO, *Guideline for clinical management of exposure to lead: executive summary.* Geneva: World Health Organization, Preventing disease through healthy environments, 2021. **Licence: CC BY-NC-SA 3.0 IGO.**
3. ANSES, *Expositions au plomb : effets sur la santé associés à des plombémies inférieures à 100 µg/L.* l'Agence nationale de sécurité sanitaire de l'alimentation, de l'environnement et du travail, 2013.
4. ANSES, *Valeurs biologiques d'exposition en milieu professionnel : Le plomb et ses composés inorganiques.* Agence nationale de sécurité sanitaire de l'alimentation, de l'environnement et du travail. Rapport d'expertise collective, 2019.
5. Bellinger, D.C., *Very low lead exposures and children's neurodevelopment.* Curr Opin Pediatr, 2008. **20**(2): p. 172-7.
6. Jusko, T.A., et al., *Blood lead concentrations < 10 microg/dL and child intelligence at 6 years of age.* Environmental health perspectives, 2008. **116**(2): p. 243-248.
7. Szigeti, T., *HBM4EU, Prioritised substance group: Lead.* National Public Health Institutes.
8. HCSP, *Détermination de nouveaux objectifs de gestion des expositions au plomb : Synthèse et recommandations.* Haut Conseil de la Santé Publique, 2014.
9. DGS, *Sites potentiellement pollués par le plomb : retours d'expérience et recommandations.* Direction générale de la santé, 2012.
10. HAS, *Intoxication par le plomb de l'enfant et de la femme enceinte : Prevention et prise en charge médico-sociale.* Agence nationale d'accréditation et d'évaluation en santé, 2003.
11. ATSDR, *Case Studies in Environmental Medicine: Lead Toxicity.* U.S. Department of Health and Human Services ; Division of Toxicology and Human Health Sciences ; Environmental Medicine Branch, 2017.
12. Barltrop, D. and F. Meek, *Effect of particle size on lead absorption from the gut.* Arch Environ Health, 1979. **34**(4): p. 280-5.
13. Garnier, R., *Toxicité du plomb et de ses dérivés.* EMC - Toxicologie-Pathologie, 2005. **2**(2): p. 67-88.
14. Markowitz, M., *Lead poisoning: a disease for the next millennium.* Curr Probl Pediatr, 2000. **30**(3): p. 62-70.
15. Barry, P.S., *A comparison of concentrations of lead in human tissues.* British journal of industrial medicine, 1975. **32**(2): p. 119-139.
16. Rabinowitz, M.B., G.W. Wetherill, and J.D. Kopple, *Kinetic analysis of lead metabolism in healthy humans.* The Journal of clinical investigation, 1976. **58**(2): p. 260-270.
17. Rabinowitz, M.B., *Toxicokinetics of bone lead.* Environ Health Perspect, 1991. **91**: p. 33-7.
18. Manton, W.I., et al., *Acquisition and retention of lead by young children.* Environ Res, 2000. **82**(1): p. 60-80.
19. Da Costa, C.P. and H. Sigel, *Stabilities of complexes formed between lead(II) and simple phosphonate or phosphate monoester ligands including some pyrimidine-nucleoside 5'-monophosphates (CMP2-, UMP2-, dTMP2-).* J Biol Inorg Chem, 1999. **4**(4): p. 508-14.
20. O'Flaherty, E.J., *Modeling normal aging bone loss, with consideration of bone loss in osteoporosis.* Toxicol Sci, 2000. **55**(1): p. 171-88.
21. Gulson, B., et al., *Revisiting mobilisation of skeletal lead during pregnancy based on monthly sampling and cord/maternal blood lead relationships confirm placental transfer of lead.* Arch Toxicol, 2016. **90**(4): p. 805-16.
22. Gulson, B., A. Taylor, and J. Eisman, *Bone remodeling during pregnancy and post-partum assessed by metal lead levels and isotopic concentrations.* Bone, 2016. **89**: p. 40-51.
23. Tellez-Rojo, M.M., et al., *Lead poisoning and marginalization in newborns of Morelos, Mexico.* Salud Publica De Mexico, 2017. **59**(3): p. 218-226.
24. Lamadrid-Figueroa, H., et al., *Biological markers of fetal lead exposure at each stage of pregnancy.* J Toxicol Environ Health A, 2006. **69**(19): p. 1781-96.

25. Rothenberg, S.J., et al., *Changes in serial blood lead levels during pregnancy.* Environmental health perspectives, 1994. **102**(10): p. 876-880.
26. Hu, H., et al., *Fetal lead exposure at each stage of pregnancy as a predictor of infant mental development.* Environmental health perspectives, 2006. **114**(11): p. 1730-1735.
27. Ettinger, A.S., et al., *Effect of calcium supplementation on blood lead levels in pregnancy: a randomized placebo-controlled trial.* Environmental health perspectives, 2009. **117**(1): p. 26-31.
28. Dalili, H., et al., *Correlation between Lead in Maternal Blood, Umbilical Cord Blood, and Breast Milk with Newborn Anthro-pometric Characteristics.* Iranian Journal of Neonatology, 2019. **10**(4): p. 6-11.
29. Al-Saleh, I., et al., *Birth outcome measures and maternal exposure to heavy metals (lead, cadmium and mercury) in Saudi Arabian population.* International Journal of Hygiene and Environmental Health, 2014. **217**(2-3): p. 205-218.
30. Rudge, C.V., et al., *The placenta as a barrier for toxic and essential elements in paired maternal and cord blood samples of South African delivering women.* Journal of Environmental Monitoring, 2009. **11**(7): p. 1322-1330.
31. Kim, S., et al., *Association between maternal exposure to major phthalates, heavy metals, and persistent organic pollutants, and the neurodevelopmental performances of their children at 1 to 2 years of age-CHECK cohort study.* Science of the Total Environment, 2018. **624**: p. 377-384.
32. Gulson, B.L., et al., *Mobilization of lead from human bone tissue during pregnancy and lactation--a summary of long-term research.* Sci Total Environ, 2003. **303**(1-2): p. 79-104.
33. Breeland G, S.M., Menezes RG, *Embryology, Bone Ossification.* n: StatPearls [Internet]. Treasure Island (FL): StatPearls Publishing, 2022.
34. Jeffery, N. and F. Spoor, *Ossification and midline shape changes of the human fetal cranial base.* Am J Phys Anthropol, 2004. **123**(1): p. 78-90.
35. Kuepfer, L., et al., *Applied Concepts in PBPK Modeling: How to Build a PBPK/PD Model.* CPT Pharmacometrics Syst Pharmacol, 2016. **5**(10): p. 516-531.
36. Wang, G.Y., et al., *Prenatal exposure to mercury and precocious puberty: a prospective birth cohort study.* Human Reproduction, 2021. **36**(3): p. 712-720.
37. Yoon, M., et al., *Assessing children's exposure to manganese in drinking water using a PBPK model.* Toxicol Appl Pharmacol, 2019. **380**: p. 114695.
38. Yoon, M. and H.J. Clewell, 3rd, *Addressing Early Life Sensitivity Using Physiologically Based Pharmacokinetic Modeling and In Vitro to In Vivo Extrapolation.* Toxicological research, 2016. **32**(1): p. 15-20.
39. Beaudouin, R., S. Micallef, and C. Brochot, *A stochastic whole-body physiologically based pharmacokinetic model to assess the impact of inter-individual variability on tissue dosimetry over the human lifespan.* Regul Toxicol Pharmacol, 2010. **57**(1): p. 103-16.
40. Lu, G., et al., *Physiologically-based pharmacokinetic (PBPK) models for assessing the kinetics of xenobiotics during pregnancy: achievements and shortcomings.* Curr Drug Metab, 2012. **13**(6): p. 695-720.
41. Coppola, P., E. Kerwash, and S. Cole, *Physiologically Based Pharmacokinetics Model in Pregnancy: A Regulatory Perspective on Model Evaluation.* Front Pediatr, 2021. **9**: p. 687978.
42. Codaccioni, M. and C. Brochot, *Assessing the impacts on fetal dosimetry of the modelling of the placental transfers of xenobiotics in a pregnancy physiologically based pharmacokinetic model.* Toxicology and Applied Pharmacology, 2020. **409**: p. 115318.
43. Brochot, C., et al., *Prediction of maternal and foetal exposures to perfluoroalkyl compounds in a Spanish birth cohort using toxicokinetic modelling.* Toxicology and Applied Pharmacology, 2019. **379**: p. 114640.
44. Leggett, R.W., *An age-specific kinetic model of lead metabolism in humans.* Environmental health perspectives, 1993. **101**(7): p. 598-616.
45. EPA, U.S., *Users Guide for the FORTRAN Version of the All Ages Lead Model.* U.S. Environmental Protection Agency, 2014.
46. Sy, M., et al., *Assessment of the Long-Term Exposure to Lead in Four European Countries Using PBPK Modeling.* Exposure and Health, 2023.

47. Tebby, C., et al., *Mapping blood lead levels in French children due to environmental contamination using a modeling approach.* Science of The Total Environment, 2022. **808**: p. 152149.
48. O'Flaherty, E.J., *Physiologically based models for bone-seeking elements: I. Rat skeletal and bone growth.* Toxicology and Applied Pharmacology, 1991a. **111**(2): p. 299-312.
49. O'Flaherty, E.J., *Physiologically based models for bone-seeking elements: II. Kinetics of lead disposition in rats.* Toxicology and Applied Pharmacology, 1991b. **111**(2): p. 313-331.
50. O'Flaherty, E.J., *Physiologically based models for bone-seeking elements: III. Human skeletal and bone growth.* Toxicology and Applied Pharmacology, 1991c. **111**(2): p. 332-341.
51. O'Flaherty, E.J., *A physiologically based kinetic model for lead in children and adults.* Environmental health perspectives, 1998. **106 Suppl 6**(Suppl 6): p. 1495-1503.
52. Turco, M.Y. and A. Moffett, *Development of the human placenta.* Development, 2019. **146**(22).
53. Caserta, D., et al., *Heavy metals and placental fetal-maternal barrier: a mini-review on the major concerns.* European Review for Medical and Pharmacological Sciences, 2013. **17**(16): p. 2198-2206.
54. Gundacker, C. and M. Hengstschläger, *The role of the placenta in fetal exposure to heavy metals.* Wiener Medizinische Wochenschrift, 2012. **162**(9): p. 201-206.
55. Goyer, R.A., *Transplacental transport of lead.* Environmental health perspectives, 1990. **89**: p. 101-105.
56. Dallmann, A., et al., *Drug Transporters Expressed in the Human Placenta and Models for Studying Maternal-Fetal Drug Transfer.* J Clin Pharmacol, 2019. **59 Suppl 1**(Suppl 1): p. S70-s81.
57. Dallmann, A., et al., *Gestation-Specific Changes in the Anatomy and Physiology of Healthy Pregnant Women: An Extended Repository of Model Parameters for Physiologically Based Pharmacokinetic Modeling in Pregnancy.* Clinical Pharmacokinetics, 2017. **56**(11): p. 1303-1330.
58. Zhang, Z., et al., *Development of a Novel Maternal-Fetal Physiologically Based Pharmacokinetic Model I: Insights into Factors that Determine Fetal Drug Exposure through Simulations and Sensitivity Analyses.* Drug Metab Dispos, 2017. **45**(8): p. 920-938.
59. Abduljalil, K., et al., *Fetal Physiologically Based Pharmacokinetic Models: Systems Information on Fetal Cardiac Output and Its Distribution to Different Organs during Development.* Clin Pharmacokinet, 2021. **60**(6): p. 741-757.
60. Zhang, Z. and J.D. Unadkat, *Development of a Novel Maternal-Fetal Physiologically Based Pharmacokinetic Model II: Verification of the model for passive placental permeability drugs.* Drug metabolism and disposition: the biological fate of chemicals, 2017. **45**(8): p. 939-946.
61. Yang, X.F., et al., *Associations between exposure to metal mixtures and birth weight.* Environmental Pollution, 2020. **263**.
62. Luecke, R.H., et al., *A physiologically based pharmacokinetic computer model for human pregnancy.* Teratology, 1994. **49**(2): p. 90-103.
63. ICRP, *Basic anatomical and physiological data for use in radiological protection: reference values. A report of age- and gender-related differences in the anatomical and physiological characteristics of reference individuals. ICRP Publication 89.* Ann ICRP, 2002. **32**(3-4): p. 5-265.
64. Brown, R.P., et al., *Physiological Parameter Values for Physiologically Based Pharmacokinetic Models.* Toxicology and Industrial Health, 1997. **13**(4): p. 407-484.
65. Black, A.J., et al., *A detailed assessment of alterations in bone turnover, calcium homeostasis, and bone density in normal pregnancy.* J Bone Miner Res, 2000. **15**(3): p. 557-63.
66. Naylor, K.E., et al., *The effect of pregnancy on bone density and bone turnover.* J Bone Miner Res, 2000. **15**(1): p. 129-37.
67. Shahtaheri, S.M., et al., *Changes in trabecular bone architecture in women during pregnancy.* Br J Obstet Gynaecol, 1999. **106**(5): p. 432-8.
68. Nashashibi, N., et al., *Investigation of kinetic of lead during pregnancy and lactation.* Gynecol Obstet Invest, 1999. **48**(3): p. 158-62.
69. Morris, M.D., *Factorial sampling plans for preliminary computational experiments.* Quality Engineering, 1991. **37**: p. 307-310.
70. Hsieh, N.H., et al., *Applying a Global Sensitivity Analysis Workflow to Improve the Computational Efficiencies in Physiologically-Based Pharmacokinetic Modeling.* Front Pharmacol, 2018. **9**: p. 588.

71. Sobol', I.M., *Global sensitivity indices for nonlinear mathematical models and their Monte Carlo estimates.* Mathematics and Computers in Simulation, 2001. **55**(1): p. 271-280.
72. Ong, C.N., et al., *Concentrations of lead in maternal blood, cord blood, and breast milk.* Arch Dis Child, 1985. **60**(8): p. 756-9.
73. Yazbeck, C., et al., *Intoxication au plomb chez la femme enceinte et le nouveau-né: bilan d'une enquête de dépistage.* Archives de Pédiatrie, 2007. **14**(1): p. 15-19.
74. Ladele, J., I. Fajolu, and C. Ezeaka, *Determination of lead levels in maternal and umbilical cord blood at birth at the Lagos University Teaching Hospital, Lagos.* PLOS ONE, 2019. **14**: p. e0211535.
75. Alemam, H., et al., *Correlation between maternal and fetal umbilical cord blood lead concentrations in Libya.* East Mediterr Health J, 2022. **28**(5): p. 345-351.
76. Bois, F.Y., *GNU MCSim: Bayesian statistical inference for SBML-coded systems biology models.* Bioinformatics, 2009. **25**(11): p. 1453-4.
77. Maszle, D. and F. Bois, *MCSim: A Monte Carlo Simulation Program.* Journal of Statistical Software, 1997. **02**.
78. R Core Team, *R: A language and environment for statistical computing. R Foundation for Statistical Computing, Vienna, Austria.* Computing, Vienna, Austria., 2022.
79. Huwaldt, J.A., *Plot Digitizer, version 2.6.9.* http://plotdigitizer.sourceforge.net, 2014.
80. Gulson, B.L., *Revision of estimates of skeletal contribution to blood during pregnancy and postpartum period.* Journal of Laboratory and Clinical Medicine, 2000. **136**(3): p. 250-251.
81. Gentry, P.R., T.R. Covington, and H.J. Clewell, *Evaluation of the potential impact of pharmacokinetic differences on tissue dosimetry in offspring during pregnancy and lactation.* Regulatory Toxicology and Pharmacology, 2003. **38**(1): p. 1-16.
82. Thépaut, E., et al., *Pregnancy-PBPK models: How are biochemical and physiological processes integrated?* Computational Toxicology, 2023. **27**: p. 100282.
83. Verscheijden, L.F.M., et al., *Physiologically-based pharmacokinetic models for children: Starting to reach maturation?* Pharmacol Ther, 2020. **211**: p. 107541.
84. Abduljalil, K., et al., *Anatomical, Physiological and Metabolic Changes with Gestational Age during Normal Pregnancy.* Clinical Pharmacokinetics, 2012. **51**(6): p. 365-396.
85. Cao, X.-L., et al., *Bisphenol A in human placental and fetal liver tissues collected from Greater Montreal area (Quebec) during 1998–2008.* Chemosphere, 2012. **89**(5): p. 505-511.
86. Mamsen, L.S., et al., *Concentrations of perfluoroalkyl substances (PFASs) in human embryonic and fetal organs from first, second, and third trimester pregnancies.* Environ Int, 2019. **124**: p. 482-492.
87. Fuentes, M., et al., *Placental effects of lead in mice.* Placenta, 1996. **17**(5): p. 371-376.
88. Griffiths, S.K. and J.P. Campbell, *Placental structure, function and drug transfer.* Continuing Education in Anaesthesia Critical Care & Pain, 2014. **15**(2): p. 84-89.
89. Loccisano, A.E., et al., *Development of PBPK models for PFOA and PFOS for human pregnancy and lactation life stages.* J Toxicol Environ Health A, 2013. **76**(1): p. 25-57.
90. Bressler, J.P., et al., *Divalent metal transporter 1 in lead and cadmium transport.* Ann N Y Acad Sci, 2004. **1012**: p. 142-52.
91. Chong, W.S., et al., *Expression of divalent metal transporter 1 (DMT1) isoforms in first trimester human placenta and embryonic tissues.* Hum Reprod, 2005. **20**(12): p. 3532-8.
92. Schramel, P., S. Hasse, and J. Ovcar-Pavlu, *Selenium, cadmium, lead, and mercury concentrations in human breast milk, in placenta, maternal blood, and the blood of the newborn.* Biological Trace Element Research, 1988. **15**(1): p. 111-124.
93. Michelsen-Correa, S., C.F. Martin, and A.B. Kirk, *Evaluation of Fetal Exposures to Metals and Metalloids through Meconium Analyses: A Review.* Int J Environ Res Public Health, 2021. **18**(4).
94. Cassoulet, R., et al., *Monitoring of prenatal exposure to organic and inorganic contaminants using meconium from an Eastern Canada cohort.* Environ Res, 2019. **171**: p. 44-51.
95. Siegers, C.P., et al., *Effect of smoking on cadmium and lead concentrations in human amniotic fluid.* Toxicology Letters, 1983. **19**(3): p. 327-331.

96. Kocyłowski, R., et al., *Evaluation of Essential and Toxic Elements in Amniotic Fluid and Maternal Serum at Birth.* Biological Trace Element Research, 2019. **189**(1): p. 45-54.
97. Neamtu, R.I., et al., *Heavy metal ion concentration in the amniotic fluid of preterm and term pregnancies from two cities with different industrial output.* Exp Ther Med, 2022. **23**(2): p. 111.
98. Thomason, M.E., et al., *Cross-hemispheric functional connectivity in the human fetal brain.* Sci Transl Med, 2013. **5**(173): p. 173ra24.
99. Thomason, M.E., et al., *Prenatal lead exposure impacts cross-hemispheric and long-range connectivity in the human fetal brain.* Neuroimage, 2019. **191**: p. 186-192.
100. Neal, A.P. and T.R. Guilarte, *Mechanisms of lead and manganese neurotoxicity.* Toxicology research, 2013. **2**(2): p. 99-114.
101. Neal, A.P., et al., *Lead exposure during synaptogenesis alters vesicular proteins and impairs vesicular release: potential role of NMDA receptor-dependent BDNF signaling.* Toxicological sciences : an official journal of the Society of Toxicology, 2010. **116**(1): p. 249-263.
102. Neal, A.P., P.F. Worley, and T.R. Guilarte, *Lead exposure during synaptogenesis alters NMDA receptor targeting via NMDA receptor inhibition.* Neurotoxicology, 2011. **32**(2): p. 281-289.
103. Rice, D. and S. Barone, Jr., *Critical periods of vulnerability for the developing nervous system: evidence from humans and animal models.* Environmental health perspectives, 2000. **108 Suppl 3**(Suppl 3): p. 511-533.
104. Guilarte, T.R., *Pb2+ inhibits NMDA receptor function at high and low affinity sites: developmental and regional brain expression.* Neurotoxicology, 1997. **18**(1): p. 43-51.
105. Ballabh, P., A. Braun, and M. Nedergaard, *The blood-brain barrier: an overview: structure, regulation, and clinical implications.* Neurobiol Dis, 2004. **16**(1): p. 1-13.
106. Laterra, J., et al., *Inhibition of astroglia-induced endothelial differentiation by inorganic lead: a role for protein kinase C.* Proc Natl Acad Sci U S A, 1992. **89**(22): p. 10748-52.
107. Bloomingdale, P., et al., *Minimal brain PBPK model to support the preclinical and clinical development of antibody therapeutics for CNS diseases.* Journal of Pharmacokinetics and Pharmacodynamics, 2021. **48**(6): p. 861-871.
108. Verscheijden, L.F.M., et al., *Development of a physiologically-based pharmacokinetic pediatric brain model for prediction of cerebrospinal fluid drug concentrations and the influence of meningitis.* PLoS Comput Biol, 2019. **15**(6): p. e1007117.
109. Sánchez-Dengra, B., et al., *Physiologically Based Pharmacokinetic (PBPK) Modeling for Predicting Brain Levels of Drug in Rat.* Pharmaceutics, 2021. **13**(9): p. 1402.
110. Ball, K., et al., *Physiologically based pharmacokinetic modelling of drug penetration across the blood-brain barrier--towards a mechanistic IVIVE-based approach.* Aaps j, 2013. **15**(4): p. 913-32.
111. Algharably, E.A., et al., *Prediction of in vivo prenatal chlorpyrifos exposure leading to developmental neurotoxicity in humans based on in vitro toxicity data by quantitative in vitro-in vivo extrapolation.* Front Pharmacol, 2023. **14**: p. 1136174.
112. Maass, C., et al., *Considering developmental neurotoxicity in vitro data for human health risk assessment using physiologically-based kinetic modeling: deltamethrin case study.* Toxicological Sciences, 2023. **192**(1): p. 59-70.
113. El-Masri, H., et al., *Integration of Life-Stage Physiologically Based Pharmacokinetic Models with Adverse Outcome Pathways and Environmental Exposure Models to Screen for Environmental Hazards.* Toxicological Sciences, 2016. **152**(1): p. 230-243.
114. Bal-Price, A. and M.E.B. Meek, *Adverse outcome pathways: Application to enhance mechanistic understanding of neurotoxicity.* Pharmacology & therapeutics, 2017. **179**: p. 84-95.

Development of a physiologically based toxicokinetic model for lead in pregnant women: the role of bone tissue in the maternal and fetal internal exposure

Ali Daoud Y[1, 2], Tebby C[1*], Beaudouin R[1, 3] and Brochot C[1, 4]

[1]Experimental toxicology and modeling unit (MIV/TEAM), Institut National de l'Environnement Industriel et des Risques, 60550 Verneuil-en-Halatte, France

[2]Péritox, UMR-I 01, University of Picardie Jules Verne, 80025 Amiens, France

[3]Sebio, Experimental and modeling unit, UMR-I 02

[4]Certara UK Ltd, Simcyp Division, Sheffield, UK

*Corresponding author: cleo.bodin@ineris.fr

Table of contents

1. Physiological parameters in mother and fetus

Table S 1: Maternal parameters related to anatomical and physiological changes during pregnancy.

Parameters	Unit	Equations [d]
Hematocrit	HCT_m (%) [a]	$HCT_0 + 0.000401 \times FA^3 - 0.0180 \times FA^2 + 0.0299 \times FA$
Cardiac output	QCG_{mp} $(L.day^{-1})$ [a]	$QCG_{m0} + 6.09 - \exp(-exp(-0.352 \times log(FA) + 1.36)) \times 24.0 \times 60.0$
Glomerular filtration rate	GFR $(L.day^{-1})$ [a]	$if\ FA < 14,\quad (-0.000294FA^4 + 0.0245\,FA^3 - 0.716\,FA^2 + 8.73FA) \times 0.001 \times 60.0 \times 24.0 + 0.113$ $if\ FA \geq 14,\quad 0.150 \times 60.0 \times 24.0$
Placental exchange surface	S_{sct} (dm²) [a]	$(20.3 \times (-0.0710 \times FA)) - 0.00659) \times 100$
Syncytiotrophoblast volume	V_{sct} (L) [b]	$(-6.83 + 0.6503) \times GA + 0.03697 \times GA^2) \times 0.001$
Syncytiotrophoblast Thickness	T_{sct} (dm) [b]	$\{0.0000195 \times FA, GA < 10.91\ \frac{V_{sct}}{S_{sct}}, GA \geq 10.91$
Volume of total blood	V_{BL} (L) [b]	$0.067 \times BWO_m + (-0.0000817 \times FA^3 + 0.003952 \times FA^2 + 0.0000841 \times FA)$
Volume of mammary glands	V_{MG} (L) [b]	$0.0123 \times e^{0.011 \times FA}$
Volume of adipose tissue	V_{AT} (L) [b]	$0.351 \times BWO_m + 0.125 \times FA$
Volume of Placenta	V_{pla} (L) [b]	$0.937 \times e^{-6.19 \times e^{-0.0813 \times FA}} - 0.00211$
Blood flow to kidneys	F_{KI} (L.day^{-1}) [a]	$\frac{QCG_{m0} \times 0.17 + (-0.0000 \times FA^4 + 0.000223 \times FA^3 - 0.00644 \times FA^2 + 0.746 \times FA) \times 24 \times}{1 - HCT_m}$
Blood flow to breast	V_{MG} $(L.day^{-1})$ [a]	$QCG_{mp} \times (0.000816 \times FA + 0.004)$
Blood flow to placenta	F_{PLM} $(L.day^{-1})$ [b]	$QCG_{m0} \times 0.005 + (0.207 \times GA + 0.0841 \times GA^2 - 0.0015 \times GA^3) \times 24$

[a] Equations were from Dallmann *et al.* [1].

[b] Equations were from Zhang *et al.* [2].

[c] QCG_{m0} and BWO_m is the cardiac output and the body weight respectively for non-pregnant woman and were calculated according to the equations of O'Flaherty [3]. HCT_0 is the hematocrit in adult and was set to 45%. *FA* is the fetal age in weeks, GA is the gestational age in weeks since the last day of the period ($FA + 2\ weeks$).

Table S 2: Fetal parameters related to physiological changes during pregnancy.

Parameters	Symbols	Equations
Hematocrit	HCT_f (%) [a]	$0.0022GA^3 - 0.163GA^2 + 4.27GA$
Cardiac output	QCG_f (L.h^{-1}) [b]	$204.043 \times \left(\frac{0.002329}{204.053}\right)^{exp\,(-0.070221FA)}$
Blood flows in the fetus [b]		
Umbilical cord	F_{UVF} (L.h^{-1})	$QCG_f \times \left(\frac{32.46133 - 0.439082FA}{100}\right)$
Ductus venous	F_{DVF} (L.h^{-1})	$F_{UV} \times \left(\frac{80.393 - 3.8122FA + 0.060133FA^2}{100}\right)$
Hepatic sinus	F_{HSF} (L.h^{-1})	$F_{UVF} - F_{DVF}$
Liver	F_{LIF} (L.h^{-1})	$F_{HAF} + F_{PVF}$
Kidneys	F_{KIF} (L.h^{-1})	$QCG_f \times \left(\frac{10.3213 - 0.12383FA}{100}\right)$
Brain	F_{BRF} (L.h^{-1})	$QCG_f \times \left(\frac{10 * exp^{(-0.5*FA)} + 4.6920FA^{0.36183}}{100}\right)$

GA is the gestation age in weeks, the time since the last day of the period, and FA the fetal age in a week. The fraction of cardiac output to the hepatic artery was set to 1%.

[a] Equations were from Zhang *et al.* [2].

[b] Equations were from Abduljalil *et a [4].*

2. Volumes of fetal organs

The volumes of fetal organs are scaled to the corresponding fraction of mass, which is defined as a normalization to the relative proportion of tissues at birth and at the end of pregnancy. As the total volume proportion of all the organs under consideration is equal to 92%, we also assumed that the fraction of the non-perfused volume is 7.98%. Fraction of mass for adrenals, brain, heart, skeletal muscle, pancreas, spleen, thyroid, kidneys, lung and liver were calculated using the following equation 2.

$$V_{organ\_fetus} = Frac_{organ\_fetus} \times WBody_{fetus} \quad \text{Eq. 1}$$

$$Frac_{organ\_fetus} = Frac_{organ\_fetus\_at\_birth} \times \frac{Frac_{organ\_fetus\_at\_birth}}{Frac_{organ\_fetus\_end\_pregnancy}} \quad \text{Eq. 2}$$

Where V_{organ_fetus} is the volume of organs in fetus in L. $Frac_{organ\_fetus}$, $Frac_{organ\_fetus\_at\_birth}$, and $Frac_{organ\_fetus\_end\_pregnancy}$ is the relative organ volume at birth and the end of pregnancy reported in Table S3. Volumes of adipose, bone and non-perfused bones are corrected by the density [3, 5].

Table S 3: Fraction of mass of fetal organs at the end of pregnancy.

Organs or tissue	Fraction of mass	Organs or tissue	Fraction of mass
Adipose tissue	0.92 - $\sum(V_{other_{tissues}})$	Bone marrow [b]	0.0138
Brain	0.347/BW_foetus_endpgy [d]	Sexual organs [b]	1.338E-3
Blood	0.0771 [b]	Pancreas [b]	0.002
Bone	0.0486 [b]	Spleen [c]	0.00330
Liver	0.04366 [c]	Thyroid [c]	0.00057
Kidneys	0.00865 [c]	Urinary tract [b]	0.0010
Skin [a]	0.061 [c]	Lung [c]	0.01746
Skeletal muscle [a]	0.207 [b]	Gut [c]	0.02607
Adrenals	0.00266 [c]	Stomach	0.0034
Mammary glands	3.2E-15 [b]	Non-perfused bone [b]	0.0857
Heart	0.00661 [c]	**Total**	**0.92**

[a] Organs lumped in the slowly-perfused compartment.

[b] Values set from the ICRP 2002 [6].

[c] Values set from the Abduljalil *et al.* [7].

[d] adapted from Luecke *et al.* [8]. BW_foetus_endpgy: foetal body weight at the end of pregnancy (kg)

Table S 4: Partition coefficients used in the p-PBPK mode based on the values from the O'Flaherty model [3].

Orangs	Partition coefficients	Organs	Partition coefficients
Kidneys	0.02	Adipose tissue	0.5
Liver	0.02	Mammary glands	0.5
Brain	0.02	Placenta	0.5
Richly perfused tissues	0.02	Slowly perfused tissues	0.5

3. Structure of bones in adult and fetus

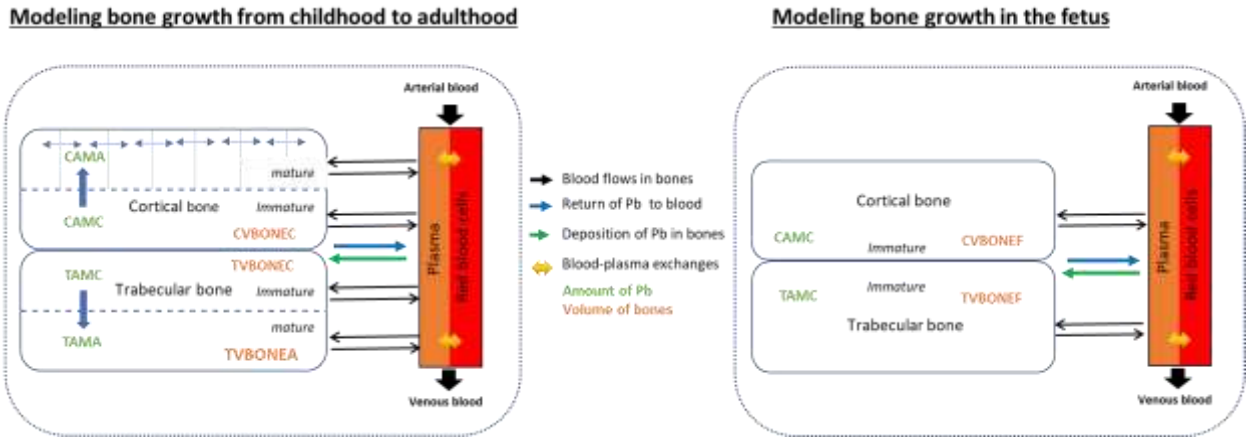

Figure S 1: Structure of bone compartments in children-adults (from brith to adulthood) and in the fetus during prenatal life.

Modeling bone growth from childhood to adulthood was based on O'Flaherty's [3] model for lead. However, some assumptions were made according to the literature information. The skeletal development in the fetus starts at the embryonic period and retained our attention for a better description of lead kinetic in the blood fetus. All bones in the fetus start as cartilage or membranes that hardens into bone (ossification process). At about 7-13 weeks of pregnancy, bone tissues start to harden under the action of calcium and phosphate. Intramembranous ossification produces the flat bones of the skull and vertebral column while endochondral ossification product the long bones of arms and legs.

Equation 5 describes the total bone formation rate during *in utero* life:

$$RVBONEF = WcBOF \times \frac{RWBODYF \times DBOF - RDBOF \times BW_f}{DBOF^2} \qquad \textit{(Eq. 2)}$$

$$BFRF = (1 + \frac{(\frac{FBFRF \times VBOF_{endP}}{RVBONEX0} - 1)}{GD} \times FA) \times RVBONEF \qquad \textit{(Eq. 3)}$$

Where $RVBONEF$ in L.day^{-1} is the derivative of bone volume in the fetus and describes the rate of change of bone volume during *in utero* life. $RWBODYF$ is the rate of change of body weight in the fetus in kg.day^{-1}. $WcBOF$ is the fraction of bone weight in the fetus during gestation. $RDBOF$ and $DBOF$ are the rate of change of bone density in kg.day^{-1}.L^{-1} and the bone density in the fetus

respectively. BW_f is the body weight of the fetus in kg. $FBFRF$ is the fraction of fetal bone formed per unit of time, set to 1642 day^{-1}, the value at birth from the O'Flaherty model. $VBOF_{endP}$ is the volume of total bone in the fetus at the end of pregnancy (L). $RVBONEX0$ and $RVBONEF$ in L.day^{-1} are the rates of change of bone in newborns and fetuses respectively. GD and FA are the gestation duration and fetal age in weeks.

4. Parameters used for the sensitivity analysis by the Morris method

Table S 5: Description of parameters included in the sensitivity analysis.

Parameters	Values	Units	Signification
BIND	2.6	mg/L	Maximum capacity of sites in red cells to bind lead
KBIND	0.006	mg/L	Half-saturation concentration of lead for binding by sites in red
G	1.2		Ratio of unbound erythrocyte lead concentration to plasma lead concentration
P0	0.015	cm/day/unit distance	Permeability constant from canaliculi to bone
D0	1,00E-07	cm/day/unit distance	Diffusion constant in bone
R0	1,00E-07	cm/day/unit distance	Permeability constant from bone to canalicule
S	0.000126	dm^2/dm	Specific canalicule surface
L	6950604555.0	cm/L of bone	Specific total canalicule length
LEAD	15000	L plasma /L bone formed	Clearance of Pb from blood to bone
CONST	0.65		Fraction of bone modeling or remodeling activity associated with trabecular bone
EXPO	0.6		Used to calculate bone volumes
VEXPO	1.188		Allometric exponent to calcuate bone volume
WEXPO	1.21		Allometric exponent to calcuate bone weight
HCT	0.45		Heamtocrit in adults
QCC	124100	L/year/Kg of BW	Cardiac output in adults
Fc_LI	0.25		Fractional blood flow to Liver
Fc_KI	0.17		Kidneys
Fc_SL	0.086		Slowly perfused tissues
Fc_BO	0.05		Bone
Fc_MG	0.004		Mammary glands
Fc_BR	0.12		Brain
Fc_AT	0.085		Adipose tissues
Fc_PLM	0.005		Maternal placenta
pInv_LI	0.02		Plasma:tissue partition coefficients for : liver
pInv_KI	0.02		Kidneys
pInv_RA	0.02		Richly-perfused tissues
pInv_PL	0.02		Placenta
pInv_BR	0.02		Brain
pInv_SL	0.5		Slowly-perfused tissues
pInv_MG	0.5		Mammary glands
pInv_AT	0.5		Adipose tissues
Vc_LI	0.0576	L/kg BW	Fractional tissue volume in adult of: liver
Vc_BLWP	0.025	L/kg BW	Blood in well-perfused tissues
Vc_KI	0.0085	L/kg BW	Kidneys
Vc_BL	0.067	L/kg BW	Blood
Vc_WP	0.16	L/kg BW	Well_perfused tissues
Vc_MG	0.0123	L/kg BW	Mammary glands
Vc_BR	0.0217	L/kg BW	Brain
Vc_AT	0.351	L/kg BW	Adipose tissues
Vc_SM	0.2917	L/kg BW	Skeletal muscle
Vc_SK	0.0383	L/kg BW	Skin
Vc_BO	0.0667	L/kg BW	Bone
Vc_RA	0.0458	L/kg BW	Richly-perfused tissues
Vc_NB	0.015	L/kg BW	Non-perfused bone
Vc_PLM	0.15159	L/kg BW	Maternal placenta
Vc_PLF	0.535	L/kg BW	Fetal placenta
Vc_IVS	0.31341	L/kg BW	Intervillous space
RCORM	0.8		Proportion of cortical bone in mother
T_sctR	0.00009	dm	Thickness of syncytiotrophoblast in placenta
KD_PL	0.01	L/dm/day	Rate of diffusion in placenta
STBR	21.5	weeks	Start of bone trunover during pregnancy
BRRP_input	0.89		Coefficient of bone turnover during pregnancy
BINDF	2.6	mg/L	Maximum capacity of sites in red cells to bind lead in fetus
KBINDF	0.006	mg/L	Half-saturation concentration of lead for binding by sites in red in fetus
GF	1.2		ratio of unbound erythrocyte lead concentration to plasma lead concentration in fetus
LEADF	15000	L plasma /L bone formed	Clearance of Pb from blood to bone in fetus
CONSTF	0.65		Fraction of bone modeling or remodeling activity associated with trabecular bone
VEXPOF	1.188		Allometric exponent to bone density in fetus
WEXPOF	1.21		Allometric exponent to bone density in fetus
Fc_HAF	0.01		Fractional blood flow in fetus: to hepatic artery
Fc_ATF	0.05		Adipose tissues
Fc_BOF	0.05		Bone
Fc_SMF	0.06		Skeletal muscle
Fc_SKF	0.01		Skin
pInv_LIF	0.02		plasma:tissue partition coefficients in fetus for: liver
pInv_KIF	0.02		Kidneys
pInv_RAF	0.02		Richly-perfused tissues
pInv_PLF	0.02		Placenta
pInv_BRF	0.02		Brain
pInv_SLF	0.5		Slowly-perfused tissues
pInv_ATF	0.5		Adipose tissues
RCORF	0.8		proportion of cortical bone in total bone

5. Distribution of parameters used for Monte Carlo simulations

Table S 6: Parameters of the p-PBPK model for Pb used in the Monte Carlo simulations.

Parameters		Distribution	Bound (min, max)
CABR	~	Gamma (9.21,11.44)	-
STBR	~	Gamma (183.36, 8.93)	-
KD_{pl}	~	LogNormal (0.0308, 3.25)	10^{-4} – 0.5
DI	~	Uniform[a]	10^{-4} – 1
BIND[c]	~	Normal (2.6, 0.26)	1.3 – 5.2
KBIND[c]	~	Normal (0.006, 6×10^{-4})	0.003 – 0.012
CONST	~	Normal (0.65, 0.065)	0.1 – 0.9
LEAD	~	Normal (15000, 1500)	7500 - 30000
RCORM	~	Normal (0.8, 0.08)	0.1 – 0.9
T_sctR	~	Normal (9×10^{-5}, 9×10^{-6})	4.5×10^{-5} – 0.00018
pInV_BRF	~	Normal (0.02, 0.002)	0.01 – 0.04
RCORF	~	Normal (0.8, 0.08)	0.1 – 0.9
VBONE_var	~	Normal (1, 0.1)[b]	0.8 – 1.2
WBONE_var	~	Normal (*VBONE*_var, 0.05)[b]	0.5 – 1.5

[a]The distribution were used only to provide prediction interval for the predicted fetal blood:maternal ratio. Otherwise, the *DI* was fixed to 3.9 µg.day^{-1}.kg^{-1}.

[b]New parameters introduced to describe variability in the volume and weight of bones in the mother and fetus.

[c]For Monte Carlo simulations BIND and KBIND were equal to BINDF and KBINDF.

6. Distribution of parameters used for Monte Carlo simulations

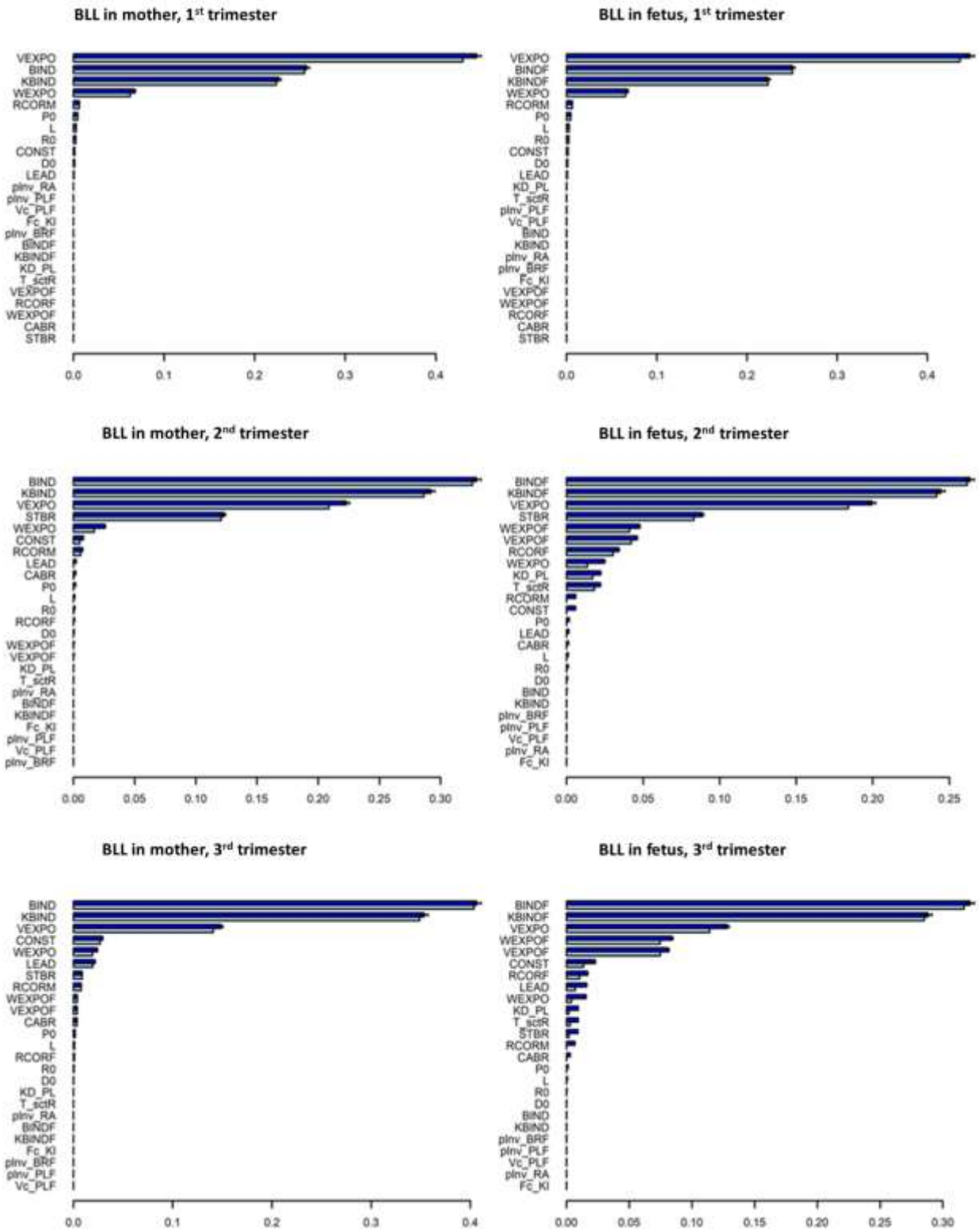

Figure S 2: FOI (light blue) and TOI (blue) from the Sobol sensitivity analysis: Pb Levels in the fetus blood and mother blood at the 1st, 2nd and 3rd trimesters of pregnancy.

7. Correlation of parameters in the p-PBPK model for lead

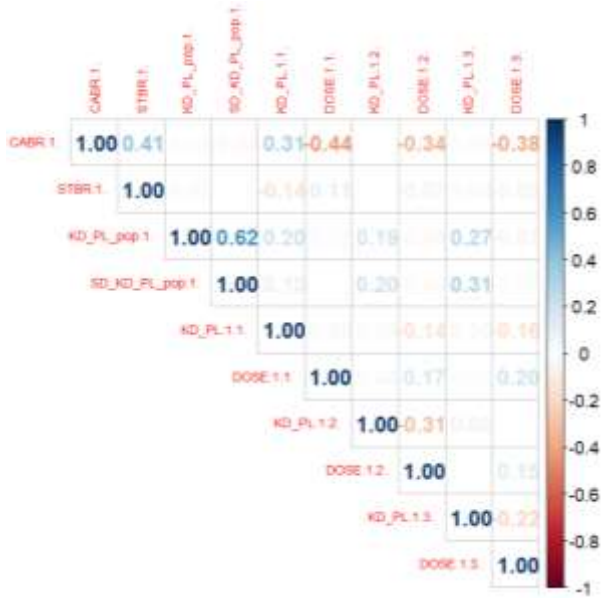

Figure S 3: Matrix of correlation coefficients for all estimated parameters by calibration.

Table S 7: Correlation of parameters after calibration

Row	Column	Correlation coefficient	p-value
CABR.1.	*STBR.1.*	0,406	0,0000
CABR.1.	*KD_PL_pop.1.*	0,030	0,1014
STBR.1.	*KD_PL_pop.1.*	0,022	0,2281
CABR.1.	*SD_KD_PL_pop.1.*	-0,044	0,0156
STBR.1.	*SD_KD_PL_pop.1.*	0,010	0,5974
KD_PL_pop.1.	*SD_KD_PL_pop.1.*	0,619	0,0000
CABR.1.	*KD_PL.1.1.*	0,315	0,0000
STBR.1.	*KD_PL.1.1.*	-0,142	0,0000
KD_PL_pop.1.	*KD_PL.1.1.*	0,205	0,0000
SD_KD_PL_pop.1.	*KD_PL.1.1.*	0,100	0,0000
CABR.1.	*DOSE.1.1.*	-0,439	0,0000
STBR.1.	*DOSE.1.1.*	0,112	0,0000
KD_PL_pop.1.	*DOSE.1.1.*	0,022	0,2208
SD_KD_PL_pop.1.	*DOSE.1.1.*	-0,002	0,9165
KD_PL.1.1.	*DOSE.1.1.*	0,047	0,0093
CABR.1.	*KD_PL.1.2.*	-0,004	0,8084

STBR.1.	*KD_PL.1.2.*	-0,002	0,9317
KD_PL_pop.1.	*KD_PL.1.2.*	0,189	0,0000
SD_KD_PL_pop.1.	*KD_PL.1.2.*	0,201	0,0000
KD_PL.1.1.	*KD_PL.1.2.*	0,038	0,0390
DOSE.1.1.	*KD_PL.1.2.*	0,044	0,0158
CABR.1.	*DOSE.1.2.*	-0,342	0,0000
STBR.1.	*DOSE.1.2.*	-0,067	0,0003
KD_PL_pop.1.	*DOSE.1.2.*	-0,042	0,0227
SD_KD_PL_pop.1.	*DOSE.1.2.*	-0,037	0,0426
KD_PL.1.1.	*DOSE.1.2.*	-0,143	0,0000
DOSE.1.1.	*DOSE.1.2.*	0,169	0,0000
KD_PL.1.2.	*DOSE.1.2.*	-0,313	0,0000
CABR.1.	*KD_PL.1.3.*	0,021	0,2414
STBR.1.	*KD_PL.1.3.*	0,038	0,0393
KD_PL_pop.1.	*KD_PL.1.3.*	0,273	0,0000
SD_KD_PL_pop.1.	*KD_PL.1.3.*	0,312	0,0000
KD_PL.1.1.	*KD_PL.1.3.*	0,049	0,0069
DOSE.1.1.	*KD_PL.1.3.*	-0,028	0,1306
KD_PL.1.2.	*KD_PL.1.3.*	0,063	0,0006
DOSE.1.2.	*KD_PL.1.3.*	0,002	0,9277
CABR.1.	*DOSE.1.3.*	-0,381	0,0000
STBR.1.	*DOSE.1.3.*	-0,065	0,0004
KD_PL_pop.1.	*DOSE.1.3.*	-0,070	0,0001
SD_KD_PL_pop.1.	*DOSE.1.3.*	-0,025	0,1724
KD_PL.1.1.	*DOSE.1.3.*	-0,162	0,0000
DOSE.1.1.	*DOSE.1.3.*	0,203	0,0000
KD_PL.1.2.	*DOSE.1.3.*	-0,001	0,9682
DOSE.1.2.	*DOSE.1.3.*	0,150	0,0000
KD_PL.1.3.	*DOSE.1.3.*	-0,217	0,0000

Bibliography

1. Dallmann, A., et al., *Gestation-Specific Changes in the Anatomy and Physiology of Healthy Pregnant Women: An Extended Repository of Model Parameters for Physiologically Based Pharmacokinetic Modeling in Pregnancy.* Clinical Pharmacokinetics, 2017. **56**(11): p. 1303-1330.
2. Zhang, Z. and J.D. Unadkat, *Development of a Novel Maternal-Fetal Physiologically Based Pharmacokinetic Model II: Verification of the model for passive placental permeability drugs.* Drug metabolism and disposition: the biological fate of chemicals, 2017. **45**(8): p. 939-946.
3. O'Flaherty, E.J., *Modeling normal aging bone loss, with consideration of bone loss in osteoporosis.* Toxicol Sci, 2000. **55**(1): p. 171-88.
4. Abduljalil, K., et al., *Fetal Physiologically Based Pharmacokinetic Models: Systems Information on Fetal Cardiac Output and Its Distribution to Different Organs during Development.* Clin Pharmacokinet, 2021. **60**(6): p. 741-757.
5. Brown, R.P., et al., *Physiological Parameter Values for Physiologically Based Pharmacokinetic Models.* Toxicology and Industrial Health, 1997. **13**(4): p. 407-484.
6. ICRP, *Basic anatomical and physiological data for use in radiological protection: reference values. A report of age- and gender-related differences in the anatomical and physiological characteristics of reference individuals. ICRP Publication 89.* Ann ICRP, 2002. **32**(3-4): p. 5-265.
7. Abduljalil, K., T.N. Johnson, and A. Rostami-Hodjegan, *Fetal Physiologically-Based Pharmacokinetic Models: Systems Information on Fetal Biometry and Gross Composition.* Clinical Pharmacokinetics, 2018. **57**(9): p. 1149-1171.
8. Luecke, R.H., et al., *A physiologically based pharmacokinetic computer model for human pregnancy.* Teratology, 1994. **49**(2): p. 90-103.